



**Utrecht  
University**

# **Classification of Coastal Dune Vegetation from Aerial Imagery with a Convolutional Neural Network**

Master thesis – Marine Sciences

Florine Kooij – 5949246

August 2022

Supervisors: prof. dr. Gerben Ruessink and dr. Jana Eichel

Utrecht University, Faculty of Geosciences, Department of Physical Geography



# ACKNOWLEDGEMENTS

Firstly, I am extremely grateful for my supervisors, prof. dr. Gerben Ruessink and dr. Jana Eichel for their support and feedback, as well as joining me on my very first fieldwork. I am also grateful for ing. Henk Markies for operating the UAV, and for ing. Marcel van Maarseveen for observing and assisting during the aerial survey and for showing me how to use a differential GPS. Furthermore, I would like to give a special thanks to ecologist Ben Kruijssen, who taught me to identify the vegetation in the Bloemendaal dunes. His knowledge of every single species – whether it be plant, moss, lichen, insect or bird – and love for nature was incredibly inspiring to me. I want to give thanks to the forest rangers of Kennemerland-Zuid as well, who gave permission to conduct a vegetation survey and a UAV survey in the National Park, and dr. Teja Kattenborn for his insight in CNN performance.

I also want to thank Winnie and my dad for joining me on during the fieldwork in the dunes, keeping me company and helping me with the equipment and search for all the different tiny plants. I am also very grateful for my dad for letting me borrow his laptop with video card and helping me optimizing some tricky bits of code. Furthermore, I want to express my appreciation for all people spending time and efforts to help strangers on the internet, whose contributions on forums like StackOverflow helped me a great deal.

Finally, I want to give many thanks to my friends and family for all their support and love, which kept me motivated during this project. Thank you, all of you.

# ABSTRACT

The Dutch coastal dunes house a rich and dynamic ecosystem with a large variation in habitats. However, they are currently threatened by geomorphological stabilization and subsequent encroachment of shrubs and tall grasses, which overtake valuable grey dune grassland. To understand such vegetation dynamics at larger scales, vegetation maps are key. While traditionally, constructing these maps from field surveys is very time- and cost-intensive, an alternative approach can be taken by training a machine learning model to classify vegetation from remote sensing data. A particularly promising model is the Convolutional Neural Network (CNN), a type of deep learning model specifically designed for pattern recognition, which has been proven highly accurate in mapping vegetation in various ecosystems. However, no vegetation mapping CNNs have been developed for coastal dune ecosystems yet.

In this thesis I present a CNN capable of mapping coastal dune vegetation on a plant community scale with an overall accuracy of 75%. The CNN has a U-net architecture and is trained for RGB orthophoto tiles with spatial dimensions of 10 by 10 m. First, a vegetation survey of the study site was conducted to better understand its vegetation, as well as an Uncrewed Aerial Vehicle survey to obtain an orthophoto and additional elevation data of the study site. The CNN was trained using 112,500 m<sup>2</sup> of manually classified vegetation maps as reference data. It was found that CNN performance per class is positively related to the surface area of that class in the reference data. Furthermore, increasing the input tile size was shown to increase overall CNN accuracy. Conversely, including elevation data as additional input information was not found to make a significant difference in CNN performance. These findings can contribute to improving the CNN further in the future.

The results of this thesis demonstrate that it is possible to use a CNN for mapping coastal dune vegetation, obtaining a vegetation map that is ecologically relevant and can be compared to other vegetation studies that use Natura 2000 habitat types. Although this CNN must still be optimized further, it could potentially be used for long-time and large-scale vegetation mapping, which could greatly improve our understanding of vegetation dynamics in coastal dune ecosystems.

# TABLE OF CONTENTS

Acknowledgements.....	2
Abstract.....	3
Table of Contents.....	4
List of abbreviations.....	6
1. Introduction .....	7
1.1. Coastal dune habitat zonation.....	7
1.2. Acceleration of encroachment.....	9
1.3. Restoring dynamics.....	9
1.4. A bird’s-eye view on vegetation .....	11
1.5. Classification with Convolutional Neural Networks.....	11
1.6. CNN classification of coastal dune vegetation.....	12
2. Theory of convolutional neural networks.....	14
2.1. Basic ANN structure .....	14
2.2. Introducing CNN.....	15
2.3. Classification per pixel .....	16
2.4. Training the CNN.....	17
2.5. CNN evaluation .....	18
3. Methods.....	19
3.1. Study site.....	19
3.2. Vegetation survey .....	20
3.2.1. Fieldwork.....	20
3.2.2. Statistical analysis .....	21
3.3. Developing the vegetation-mapping CNN .....	21
3.3.1. UAV survey.....	21
3.3.2. Reference data generation .....	22
3.3.3. Preparation of the CNN training and evaluation dataset .....	24
3.3.4. The CNN architecture and hyperparameters.....	24
3.3.5. Training the CNNs .....	25
3.3.6. Evaluating the CNNs.....	26
3.3.7. Using the CNN to make vegetation maps .....	26

4.	Results.....	27
4.1.	Vegetation survey .....	27
4.2.	CNN performance for different input data types .....	30
4.3.	Class-based and spatial patterns in CNN performance .....	30
4.4.	CCN-based vegetation classification of the full study area .....	32
5.	Discussion.....	35
5.1.	Mapping coastal dune vegetation with CNN .....	35
5.2.	The coastal dune vegetation in the Bloemendaal blowout complex .....	35
5.2.1.	The main vegetation classes .....	35
5.2.2.	Translation from vegetation to CNN classes.....	36
5.2.3.	The blowout complex' vegetation map and vegetation distribution .....	37
5.3.	Effects of additional input data on CNN performance .....	38
5.3.1.	Elevation data as extra information.....	38
5.3.2.	Alternatively: cross-shore distance data as extra information.....	38
5.4.	Effects of input tile size on CNN performance.....	39
5.5.	CNN performance per class .....	39
5.5.1.	General remarks.....	39
5.5.2.	Privet .....	40
5.5.3.	Other vegetation and terrain types .....	40
5.6.	Outlook .....	41
5.6.1.	Combining CNN vegetation mapping with vegetation surveys in the field .....	41
5.6.2.	Potential further CNN applications.....	41
6.	Conclusion.....	43
	References .....	44
	Appendix .....	51
	Appendix A: List of species observed during the vegetation survey .....	51

# LIST OF ABBREVIATIONS

<b>ANN</b>	Artificial Neural Network
<b>CNN</b>	Convolutional Neural Network
<b>DEM</b>	Digital Elevation Model
<b>DGPS</b>	Differential Global Positioning System
<b>GCP</b>	Ground Control Point
<b>NMDS</b>	Non-metric Multidimensional Scaling
<b>NPZK</b>	National Park Kennemerland-Zuid
<b>ReLU</b>	Rectified Linear Unit
<b>RGB</b>	Red, Green and Blue
<b>RHD</b>	Rabbit Hemorrhagic Disease
<b>RMSE</b>	Root Mean Square Error
<b>UAV</b>	Uncrewed Aerial Vehicle

# 1. INTRODUCTION

The Dutch coastal dunes stretch out over 350 km along the coastline of the Netherlands, from the sandy beaches of the North Sea to up to a few kilometers inland (Fig. 1). The dunes, which are typically between 10 and 50 m high (Arens, Slings, et al., 2013), house a rich and dynamic ecosystem and have high societal relevance. Since approximately 9 million people in the Netherlands live in regions that lie below sea level (Mulder et al., 2011), water safety is one of the main priorities of Dutch water management, and the dunes are a major part of the primary coastal defense (Rijksoverheid, 2021). The dunes also offer a space for recreation and tourism, and are used to supply drinkwater to the densely populated areas beyond the dunes (Grootjans et al., 2004).

Besides these important services, the coastal dunes also have a large ecological value. They contain a wide range of different habitat types, including white and grey dune, heather, shrub, dune slacks and woodlands (Doing, 1995), which results in high biodiversity as well. Although the dunes cover only ca. 1% of the total surface area in the Netherlands, over half of all vascular plant species present in the Netherlands can be found in the dunes (Heslenfeld et al., 2008). They are also home to many (endangered) Red List species (e.g. Grootjans et al., 2004).

## 1.1. Coastal dune habitat zonation

The Dutch coastal dune ecosystem is characterized by strong coast-to-inland gradients in abiotic factors such as wind strength, sand burial, soil salinity and nutrient availability, which result in a clear zonation in dune vegetation (Marcenò et al., 2018). The zonation results in different habitats along a successional gradient, schematically represented in Fig. 2. It should be noted that in reality, the abiotic and ecological gradients are mostly found in non-linear, small-scale patterns (Doing, 1995), creating a varied patchwork of microhabitats. The main coastal dune habitats are also included in the Natura 2000 network, a European Union-wide network of protected nature areas (see e.g. Evans, 2012).

Close to the shoreline, the environmental conditions are too harsh for plants. When moving from the shoreline inwards, the first vegetation can be found on the backshore in places where washed up organic material (driftwood, macroalgae) provides nutrients. Only a few specialized halophytes, such as *Cakile maritima* and *Elymus farctus* subsp. *boreo-atlanticus*, are adapted to withstand the local increased salinity



Figure 1: Coastal dune distribution in the Netherlands (blue). The red dot marks the location of the study site.

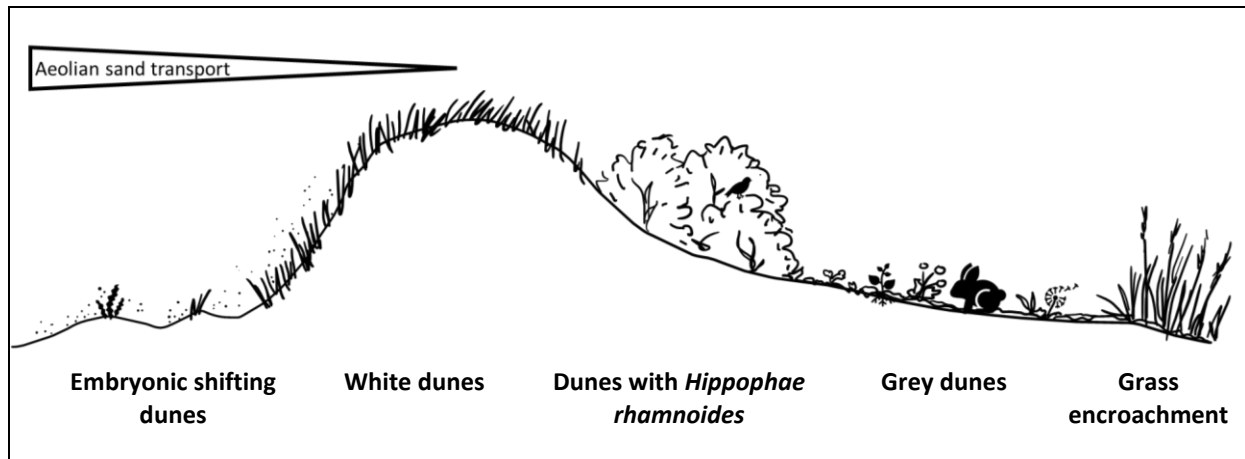


Figure 2: Schematic of successive vegetation phases in dry dunes with a continuous foredune. Note that these are not true proportions. Aeolian sand transport from the beach is indicated with an arrow.

and instability due to water and sand dynamics (Clausing et al., 2000). In the Natura 2000 network, this habitat is referred to as the ‘embryonic shifting dunes’ (H2110).

Beyond the beach lies the foredune, typically covered with the pioneer grass marram (*Calamagrostis arenaria*<sup>1</sup>). In the Natura 2000 network, this habitat is referred to as the ‘young’ or ‘white’ dunes (H2120). The high burial rates due to aeolian sand deposition, and increased salinity due to salt spray, cause this habitat to be quite poor in species as well. For marram, however, sand burial stimulates growth, and hereby increases marram’s capacity to capture the deposited sand and stabilize the dune (Maun, 1998; Zarnetske et al., 2012). In this way, the foredune is shaped through a feedback mechanism between the geomorphic conditions and ‘dune-building’ vegetation. In other words: the coastal dune landscape is a biogeomorphic ecosystem (Corenblit et al., 2007, 2015). While vegetation growing seaward of the foredune is generally adapted to withstand burial, and captures sand simply by forming an obstacle for aeolian sand transport, marram is especially efficient at capturing sand (Zarnetske et al., 2012).

Further inland, where sand accumulation rates are lower, grey dunes (H2130) can develop. This habitat type has a very high species richness, with several associated vegetation communities consisting mainly of herbs, mosses and (particularly in lime-poor areas) lichen, alternated by patches of bare sand (Isermann, 2011). The high plant richness leads to a high overall biodiversity, with many characteristic butterflies, grasshoppers and other insects which are, in turn, a source of food for higher trophic levels (e.g. Van Til & Kooijman, 2007). According to the European Habitats Directive, the grey dunes are a priority habitat type (Council of the European Commission, 1992).

The grey dunes are sustained by disturbances such as burial and rabbit activities, which keep the landscape open (e.g. Isermann et al., 2010). If those disturbances disappear, the dunes stabilize further, and encroachment of grasses like *Carex arenaria* and *Calamagrostis epigejos* and shrubs like *Hippophae rhamnoides* (sea buckthorn) can take place. Although dunes with *Hippophae rhamnoides* (H2160) are a

<sup>1</sup> In this thesis, species names of vascular plants are based on *Heukels’ Flora van Nederland* 24<sup>th</sup> edition (Duistermaat, 2020). In previous editions of this flora, and in much of the scientific literature, marram is referred to as *Ammophila arenaria*.



valuable habitat type in their own right, offering shelter and berries for birds breeding in the dunes (Verstrael, 1996), expansion of buckthorn can cause a decrease in species richness that includes the loss of rare taxa of grey dune species (Isermann et al., 2007). Similarly, grass encroachment is also associated with low species diversity and richness (Veer & Kooijman, 1997).

## **1.2. Acceleration of encroachment**

Up to the 1980s, most of the Dutch coastal dunes were fully geomorphologically stabilized and covered by vegetation. This resulted in pioneer stages becoming increasingly rare and grass and shrub encroachment increasing, threatening the high dune biodiversity (Arens, Mulder, et al., 2013). This development was caused by a number of factors amplifying each other.

First of all, due to the low elevation of most of the Netherlands, the coastal dunes have been strengthened so much that the foredunes began to resemble dikes: tall, stable and continuous. Records of marram planting to stabilize and strengthen the foredune go back to the 14<sup>th</sup> century (Oost et al., 2012). As a result, aeolian sand transport from the beach to beyond the foredune ceased entirely in many places (e.g. Arens, Mulder, et al., 2013; Ruessink et al., 2018).

Additionally, two viral epidemics in European rabbits (*Oryctolagus cuniculus*), myxomatosis in the 1950s and rabbit hemorrhagic disease (RHD) in the 1990s, nearly eradicated rabbits in Europe. Together, they caused a decrease of over 90% in population (Drees, 2004; Provoost et al., 2011). Directly after the myxomatosis outbreak, grass and shrub encroachment accelerated: there were barely any rabbits left to destabilize the landscape (Provoost et al., 2011; van der Hagen et al., 2020).

On top of that, atmospheric nitrogen (N) began to accumulate in the dunes. Deposited atmospheric nitrogen consists mainly of nitrogen oxides (NO<sub>x</sub>) from the burning of fossil fuel and ammonia (NH<sub>4</sub>) from agriculture (Kooijman et al., 2021). Different habitats have different thresholds for nitrogen, above which the habitat deteriorates. Grey dunes in particular are highly sensitive to nitrogen deposition (van Dobben et al., 2014), which has been found to further accelerate grass encroachment (e.g. Kooijman et al., 2017; Veer, 1997).

## **1.3. Restoring dynamics**

In the 1980s, a paradigm shift in how coastal defense and the coastal dune ecosystem should be managed took place. As dunes were overgrown by shrubs and grasses, dynamical dunes became the new ecological aspiration. Instead of strengthening the foredune with marram, coastal defense started focusing on sand supply, through large-scale beach and shoreface nourishments. As a result, foredunes began accreting more sand, and previous retreat of the coastline stopped (Arens, Slings, et al., 2013). At the same time, experiments with new management strategies started to restore aeolian dynamics and combat grass and shrub encroachment.

A first strategy to combat encroachment was the removal of grass and shrubs through mowing, topsoil removal or shallow sod cutting, to create space for grey dune vegetation to return. Van Til & Kooijman (2007) found that shallow sod cutting, where ca. 5 cm of top soil is removed, was very effective in restoring the grey dune landscape. In a field experiment in the Amsterdam Water Supply Dunes, they found that cut areas developed into a diverse habitat, with bare sand, herbaceous vegetation and moss patches, within a few years. Furthermore, they found that these areas also attracted rabbits, butterflies and grasshoppers, including several characteristic or Red List species (Van Til & Kooijman, 2007).

In combination with mechanical vegetation removal, steps to increase grazing pressure were taken as well. Several studies have shown the positive effects of grazing on grey dune vegetation richness (Hewett, 1985), mitigation of grass and shrub encroachment (Lamoot et al., 2005) and butterfly populations (WallisDeVries & Raemakers, 2001). Complimenting the introduction of great grazers like cattle and horses to the dunes, rabbit populations have been recovering naturally since 2003, when resistance against RHD began to rise (IJzer et al., 2016).

A final measure to promote aeolian dune dynamics is the creation of artificial blowouts (Schwarz et al., 2019). In dynamic coastal dunes, blowouts are a naturally occurring erosional feature. There are two main types, saucer and trough blowouts. Both types consist of a deflation basin with erosional walls, where sand is removed, and a depositional lobe, where sand accumulates (Hesp, 2002). Trough blowouts in the foredune are wind-driven and connect the beach to the backdunes, forming a passage for aeolian sand transport beyond the foredune. On the other hand, saucer blowouts develop on dune crests and are mainly governed by the availability of bare sand (Schwarz et al., 2019).

Particularly the creation of artificial foredune blowouts have proved to be an effective and sustainable measure in restoring dune dynamics (Schwarz et al., 2019). One successful implementation can be found in National Park Zuid-Kennemerland (NPZK) near Bloemendaal, where five foredune notches were excavated in 2012 and 2013 to increase habitat diversity and mitigate biodiversity loss inwards of the foredunes (Fig. 3) (Kuipers et al., 2016). In the following years, Ruessink et al. (2018) observed sand deposition over 100 m inlands of the blowout complex, indicating their large-scale geomorphological impact. Since the excavation, ca. 75% of all wind-transported sand has been deposited beyond the foredune, while before that time all sand remained seawards of the foredune. This shows the high effectiveness of the blowout complex in facilitating aeolian transport into the backdunes (Ruessink et al., 2018).

The ecological impact of blowouts has not been extensively studied yet. Hesp stated in 1991 that the stress blowouts impart on the surrounding landscape can increase the abundance of pioneer species of early successional stages. He also noted that when a blowout is eroded down to the water table and erosion ceases, a species-rich dune slack could develop (Hesp, 1991). A study by Van Boxel et al. (1997) found that in the three years after the creation of a number of artificial saucer blowouts in the Midden Heerenduin dunes near Haarlem, the species composition of moss patches in the deposition area shifted from the burial-intolerant *Campylopus introflexus* and *Hypnum cupressiforme* towards the burial-tolerant *Hypnum cupressiforme*. They did not observe any indications that shrubs or marram were (negatively)



**Figure 3: The foredune notches of the Bloemendaal blowout complex, seen from the beach. Photo taken in March 2022.**

affected by the blowouts' deposition (Van Boxel et al., 1997). Finally, in a study by Laporte-Fauret et al. (2021) focusing on two artificial foredune notches in southwest France during one year, found a positive relation between disturbance through sand deposit and species richness, contradicting theoretical ecology models. The authors hypothesized that the increase in species richness was due to an increase in ruderal plant species while stress-tolerant pre-blowout vegetation was still surviving burial, and they expected that over longer timescales, species richness would decrease again (Laporte-Fauret et al., 2021).

#### **1.4. A bird's-eye view on vegetation**

Although these studies offer some insight, much is still unknown about the large-scale response of coastal dune vegetation dynamics to abrupt changes in the abiotic environment, such as artificial blowout creation. For a good scientific understanding of these vegetation dynamics, as well as good dune management, it is important to monitor the distribution and surface area of the different coastal dune habitats. To do so, vegetation maps are an invaluable tool, since they can provide an overview of the habitat composition of an entire landscape at a glance. Well-known vegetation maps for the Dutch coastal dunes includes the 1:50,000 vegetation map for the entire Dutch coast by Doing (1988), compiled over a period of ca. 13 years, and the Dutch Natura 2000 habitat type map, assembled from over 100 smaller-scale maps by AERIUS (part of the RIVM, the Dutch National Institute for Public Health and the Environment). The latter vegetation map is updated regularly and is used to compute nitrogen deposition excesses in Natura 2000 regions.

Traditionally, the vegetation data required to create such vegetation maps is obtained by surveying the target area's vegetation in the field (Pedrotti, 2012). However, this method is both time-consuming and expensive, which limits its use in monitoring areas on longer timescales and at larger scales. In recent years, advancements in remote sensing technology and machine learning algorithms have given rise to more efficient methods of creating vegetation maps, in which self-learning algorithms are trained to classify vegetation from remote sensing data (Xie et al., 2008). These methods eliminate the need for extensive field surveys.

For coastal dune ecosystems, such methods have yielded high classification accuracies for vegetation classification using a maximum likelihood classification algorithm (Suo et al., 2019) and a Support Vector Machine (Medina Machín et al., 2019), with overall accuracies of respectively 78% and 88%. However, these results were achieved using multispectral UAV-data, which requires specialistic sensors to obtain – as such, data collection is more expensive and not much multispectral aerial imagery is publicly available, limiting the applicability of these methods. On the contrary, high resolution RGB (red, green and blue) aerial imagery is both less expensive to collect, because there are no extra sensors required, and often already accessible. For example, annual RGB orthophotos of the entire Netherlands with a resolution of 25 by 25 cm (since 2016) and 8 by 8 cm (since 2021) are publicly available via PDOK (pdok.nl).

#### **1.5. Classification with Convolutional Neural Networks**

One promising technique in vegetation classification is the use of a Convolutional Neural Network (CNN), a type of artificial intelligence capable of analyzing patterns in images and hereby recognizing individual plant species and communities (Kattenborn et al., 2021). In short, a CNN can be trained to map vegetation by showing it input data (like an orthophoto) along with the desired output data (a vegetation map). Once it has learned to produce accurate vegetation maps itself, it can be used in further applications.

Due to hardware memory restrictions, orthophotos of larger regions are typically divided into small tiles, which the CNN can process separately. Previous studies have found that increasing tile size can improve

CNN performance (Kattenborn et al., 2020; Nevavuori et al., 2019). Furthermore, in addition to the orthophoto, extra information can be included in the input data as well. Specifically, several studies have included elevation in their CNN's input data, with mixed results: some studies observed no clear improvement in CNN performance when including elevation (Kattenborn et al., 2020; Nezami et al., 2020), whereas Sothe et al. (2020) found that including elevation significantly increased CNN performance. This could indicate that the effectiveness of including elevation to increase CNN performance depends on the specific conditions and methods of a study.

Vegetation-aimed CNNs have been applied successfully in a wide range of landscapes, such as forests, glacier foreland, rice paddies, wetlands, urban areas, and farmland with crops (Kattenborn et al., 2021). Several studies have shown that CNNs outperform common shallow learning approaches such as Random Forest, Support Vector Machine and XGBoost for remote sensing vegetation classification tasks (e.g. Ayrey & Hayes, 2018; Barbosa et al., 2020; Guidici et al., 2017; Hartling et al., 2019; Knauer et al., 2019; Liao et al., 2020; Rezaee et al., 2018; Zhang et al., 2018; Zhong et al., 2019). Additionally, high quality CNN-based vegetation classification can be performed with only RGB orthoimagery, without requiring multispectral or hyperspectral data (Kattenborn et al., 2021).

To my knowledge, CNN has not yet been applied successfully to classify vegetation in coastal ecosystems. A study on land cover classification set in the San Francisco Bay Area (USA) by Guidici et al. (2017) included 'dune vegetation' as class, but their CNN yielded a class accuracy of 0.0%. A similar study, conducted in the Danube Delta (Romania) by Niculescu et al. (2018), included 'dunes (sand)' and 'dunes (vegetation)' as classes. For these classes their CNN yielded F-scores of respectively 0.32 and 0.22 on a scale from 0 (worst) to 1 (best). Both studies were focused on a larger area than just coastal dunes, which could explain the low CNN performance. Neither of them attempted to differentiate between different coastal dune vegetation types (Guidici et al., 2017; Niculescu et al., 2018).

## **1.6. CNN classification of coastal dune vegetation**

In order to gain a better understanding of large-scale and long-term vegetation responses to abrupt disturbances such as blowout excavation and to assess the effectiveness of coastal dune management measures, vegetation monitoring is essential. To monitor this response, vegetation maps should be generated for multiple years to track vegetation development over time. However, traditional methods of obtaining these maps are time- and cost-expensive, making them unsuitable for this purpose. Therefore, a CNN is considered as faster and more accessible option.

This thesis' aim is to develop a CNN able to classify coastal dune vegetation from high-resolution aerial RGB imagery. The Bloemendaal blowout complex has been selected as study site, because of the blowouts' geomorphological importance and the availability of high resolution orthophotos for each year since 2013. The study consists of a vegetation survey, to gain an understanding of the ecosystem at the species- and community level, a UAV-survey to obtain recent high resolution aerial imagery and the development of a CNN able to classify the vegetation from this imagery. To better understand the vegetation of the study site, and to assess to what extent a CNN is able to classify this vegetation, four research questions will be answered:

- Which vegetation classes can be distinguished in a coastal dune ecosystem, and how well does a CNN distinguish these?
- To what extent does inclusion of elevation data as extra input data affect CNN performance?
- To what extent does the input of different orthophoto tile dimensions affect CNN performance?

- Which factors affect the CNN classification performance of different coastal dune vegetation classes?

In the next chapter, an overview of CNNs and their inner workings will be given. Next, in the Methods chapter, the study site will be introduced, as well as the methodology of the vegetation survey and CNN development. The findings of this thesis will then be presented in the Results chapter, including the vegetation map obtained by CNN classification from aerial imagery. The results will be discussed and put in a wider context in the Discussion. Finally, the Conclusion will review what was achieved in this thesis and provide an outlook for further research.

## 2. THEORY OF CONVOLUTIONAL NEURAL NETWORKS

A CNN is a special type of Artificial Neural Network (ANN), a digital network modelled after the nervous system's natural neural network. The strength of these ANNs is that, when faced with a problem, they are able to learn how to solve that problem through training (Shrestha & Mahmood, 2019). In that way, they behave similar to a mammalian brain – albeit much, much simpler (for now). There are many different types of ANN, for a wide range of applications: for instance, image and speech recognition, translation, question answering and predicting drug molecule activity (Lecun et al., 2015). However, despite the high number of different specializations, the basis of these ANNs is often quite similar.

### 2.1. Basic ANN structure

The most basic unit in an ANN is the node, or neuron (Fig. 4). Nodes work similar to mathematical functions: they take one or multiple inputs, perform some type of computation and then return one or multiple outputs. After the node operation, a non-linear activation function is performed that determines whether the node is switched on or off, by transforming the output into a given range. The non-linearity of activation functions allows for learning complex patterns. One of the most common activation functions is a ReLU (Rectified Linear Unit) which can be expressed as follows (Lin & Shen, 2018):

$$f(x) = \begin{cases} x, & \text{if } x \geq 0 \\ 0, & \text{if } x < 0 \end{cases}$$

A neural network is built up of interconnected nodes, with nodes performing the same operation grouped together in layers. The first ANNs had an architecture, or internal node structure, consisting of one layer. More recently, 'deep learning' neural networks were conceived, networks with hidden layers between the input and output layer to enable them to perform more complex analyses on the original input (Lecun et al., 2015). In a feedforward neural network, such as the one used in this thesis, information can only flow in one direction from input to output, without looping back to previous layers (see Fig. 4) (Shrestha & Mahmood, 2019).

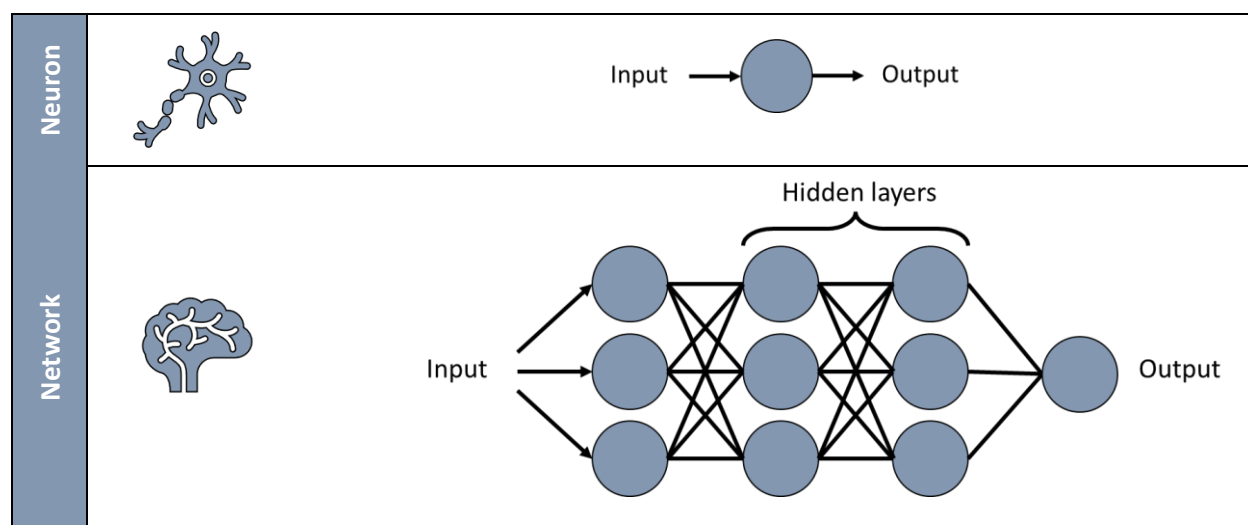


Figure 4: Basic structure of a single neuron (node) and an artificial neural network.

There are multiple ways to connect the network's layers: for instance, one could choose a 'fully-connected' approach and connect all nodes in a layer to all nodes of a previous layer (as shown in the schematic ANN in Fig. 4). The downside of this approach is its inefficiency and its proneness to overfitting (LeCun et al., 1990).

## 2.2. Introducing CNN

In 1990, LeCun et al. presented the first CNN: a new type of neural network, able to recognize handwritten digits from zip codes on envelopes. Instead of a fully-connected network, this network was locally connected: since it was developed especially for pattern recognition in images 'shortcuts' were used for a better performance. More specific, the network could extract local feature information to classify the digits. For example, a 1, 4 and 7 all contain a diagonal line slanted forwards in some location, and a 2, 4, 5 and 7 all contain a vertical line. The network detects these types of local features using convolution; the base operation in all CNNs (LeCun et al., 1990).

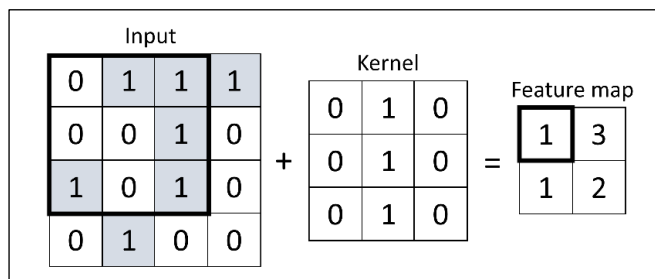


Figure 5: Example of a convolution operation. Note that although in this example only 0s and 1s are used for simplicity, this does not need to be the case in real CNNs. The bold squares indicate the kernel location on the input matrix and the corresponding cell in the output feature map.

An example of convolution is shown in Fig. 5. For a convolution, specific features in the input data are detected using a kernel, or filter, and then stored in a feature map. In this case, the input is the a  $4 \times 4$  matrix that represents the letter J. The kernel is a  $3 \times 3$  matrix that contains a weight in each cell. In this case, the weights are chosen such that the kernel can detect vertical lines in the input data. For an  $n \times n$  input matrix, the output feature map has a size of  $(n - 2) \times (n - 2)$ .

During the convolution, the kernel is superimposed on the input matrix, and the dot product of the kernel and the kernel-'covered' part of the input matrix is calculated. The resulting value is stored in the feature map at the kernel location. The process is repeated for each possible kernel position on the input matrix, filling the feature map. In Fig. 5, the feature map indicates the presence and position of vertical lines in the input matrix: there is a vertical line in the top right. A feature map for a specific feature can be used as input in another convolution layer, allowing for 'deeper' pattern recognition.

Besides convolution layers, information can be 'downsampled' by being passed through pooling layers, which reduce the spatial dimensions of the information. The most common type of pooling operation is max pooling. In this thesis,  $2 \times 2$  max pooling with stride 2 is used, as shown in Fig. 6: a  $2 \times 2$ -sized part of the input matrix is selected, starting in a corner; for this part, the highest value is stored in an output matrix. The selection shifts two cells (stride 2) to the right and the process is repeated. At the end of the row, the selection shifts two cells down and the process is repeated for another row, until the entire input matrix has been pooled into the output layer.

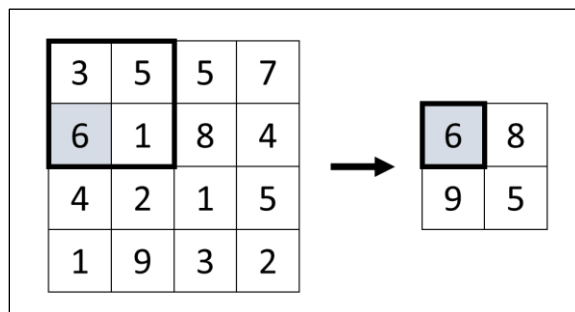


Figure 6: Example of max pooling operation with stride 2.

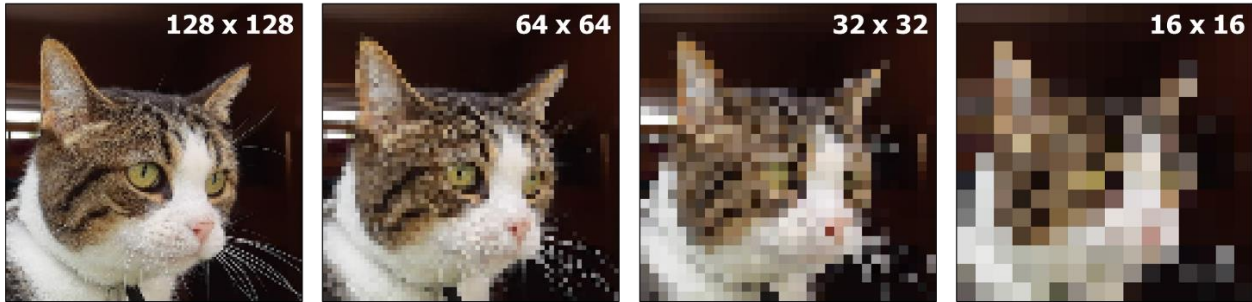


Figure 7: Photo of a cat with different pixel resolutions.

The benefit of pooling layers is that through reducing the resolution of the input information, convolution layers can detect higher-level features. For example, consider applying a  $3 \times 3$  convolution to the photo of a cat shown in Fig. 7 in different resolutions. At a resolution of 128 by 128 pixels, a  $3 \times 3$  convolution can detect small-scale features, such as whiskers. By reducing the image’s resolution, a  $3 \times 3$  convolution can detect larger features such as triangular ears. By combining the features from different levels, the CNN can make a more accurate classification.

### 2.3. Classification per pixel

The first CNNs all returned one classification per image, e.g. “cat” if the image showed a cat. For vegetation classification from aerial imagery, however, one image can contain multiple classes (e.g. “sand”, “water” and “trees”), and therefore one classification per image becomes insufficient. In 2015, Ronneberger et al. presented a solution for this: the U-net architecture, which enables segmentation: classification per pixel instead of per image.

In this thesis, a U-net architecture is used, shown in Fig. 8. Rectangles represent feature maps, and arrows represent layer operations. The spatial dimensions of the feature maps are displayed at their sides, the number of (feature) channels is displayed above the feature maps. The input for the U-net (top left) is an

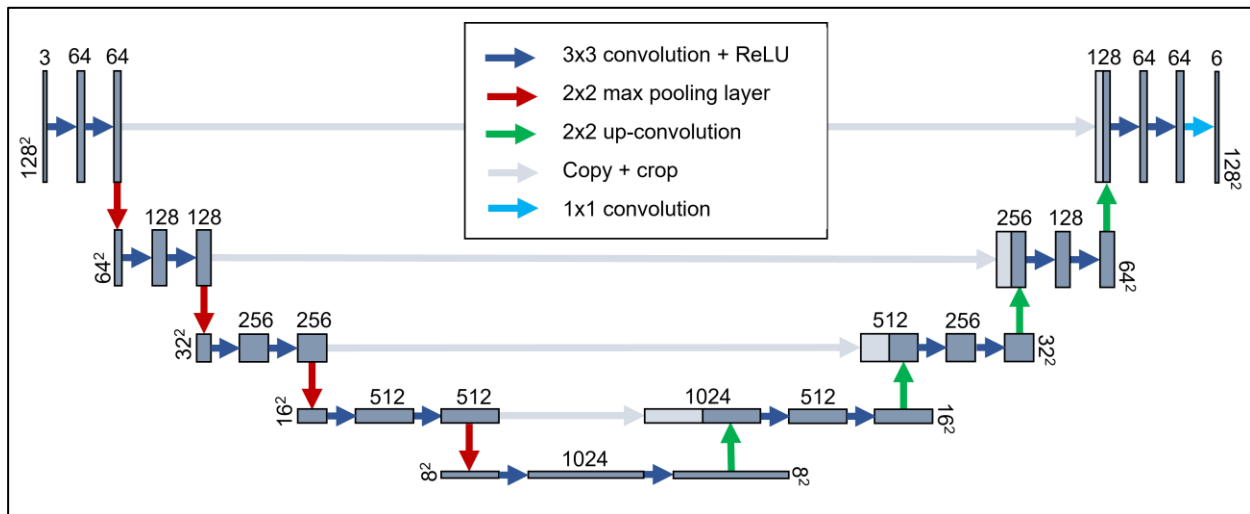


Figure 8: Schematic view of the U-net architecture (Ronneberger et al., 2015). Each rectangle represents a feature map, with spatial dimensions indicated at the side and number of channels indicated above the rectangle. Layer operations are indicated with colored arrows. The input (top left) is an RGB orthophoto tile of 128 by 128 pixels and 3 channels (RGB). The output (top right) has the same spatial dimensions as the input, but has 6 channels, one for each class.



RGB image (3 channels) of 128 by 128 pixels. The output has the same spatial dimensions, but has a channel for each class the CNN aims to detect – in this case 6 channels. The layers of the U-net architecture are arranged in a contracting path (downwards) and an expansive path (upwards), making the full architecture U-shaped (Ronneberger et al., 2015).

In the contracting path, features are extracted from the input at increasingly high levels by repeated  $3 \times 3$  convolutions followed by a ReLU, and downsampling through  $2 \times 2$  max pooling layers with stride 2. In the expansive path, localization is implemented through ‘up-convolution’ which essentially maps features to pixels. An up-convolution combines ‘upsampling’ (Fig. 9), where spatial dimensions are increased again, with a  $2 \times 2$  convolution halving the number of feature channels. This feature map is then concatenated with the corresponding feature map from the contractive path, to combine features at different levels. For pixels close to the border, missing input data required for max pooling is retrieved by mirroring (Ronneberger et al., 2015).

The last layer of the network performs a  $1 \times 1$  convolution, which serves to transform the information from the feature channels into a classification for each class. An output activation function is applied to transform the output into a specific range for further analysis (Ronneberger et al., 2015).

## 2.4. Training the CNN

CNNs are trained through ‘supervised learning’, where the network is trained using a dataset of input data combined with pre-classified reference data (Alloghani et al., 2020). During the training phase, the weights of the convolution kernels are optimized to minimize the difference between the model’s classification and the reference data, expressed in a ‘loss function’. This is achieved with a backpropagation learning algorithm (Mizutani, 1994). To minimize the loss function, several optimizer algorithms can be used, all with their own strengths and applications (Kingma & Lei Ba, 2015).

For the training of the model, the reference dataset is typically split in three parts: a training set, a testing set and an evaluation set. The evaluation set is put aside and not used for training, to be able to evaluate the CNN with unfamiliar data. The training and testing set are both used for training: weight optimization is performed using the training set, and the testing set is used to evaluate how the model performs on unfamiliar data for each pass of the full training set through the CNN (‘epoch’). If the CNN is trained for too many epochs, or if the training dataset is too small, the model can start overfitting (Fig. 10): the accuracy for the training dataset keeps increasing because the model learns features highly specific to the training dataset, but as a result the accuracy for the testing dataset decreases.

Typically, the training data is passed through the model in ‘batches’ instead of all data at once. After each batch, model parameters are updated. Small batches require less system

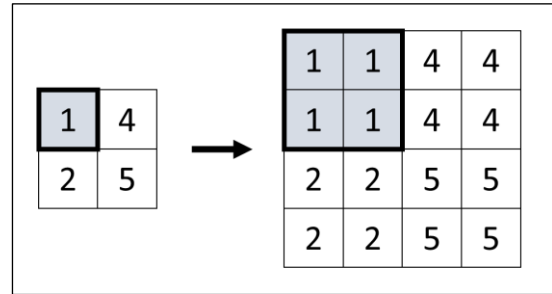


Figure 9: Example of upsampling of a  $2 \times 2$  matrix.

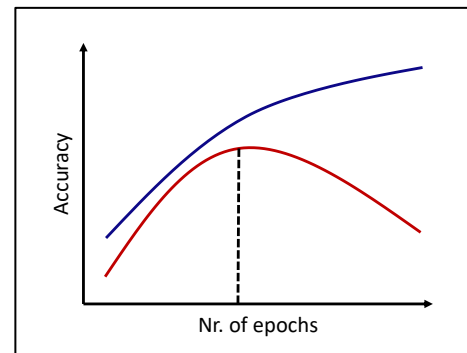


Figure 10: Schematic model of training set accuracy (blue) and test set accuracy (red) during CNN training. The dashed line indicates the optimal number of epochs – beyond that number, the model starts to overfit.

memory, an important limitation for large datasets, and since the model parameters are updated more frequently the model learns faster. However, small batch sizes do lead to a longer computation time per epoch, and because data in small batches can be uneven the model does, so to speak, not always learn in the right direction.

While the CNN’s parameters, such as the kernel weights of the convolution operations, are altered by training, the CNN also has intrinsic settings that remain unchanged throughout the training process. These settings, such as the used loss function, optimizer, number of epochs and batch size, are called ‘hyper-parameters’.

## 2.5. CNN evaluation

Before applying the trained CNN to real-life problems, its performance should be evaluated on the evaluation set not used during training. There are several common metrics to assess CNN performance, as discussed by Kattenborn et al. (2021). For this thesis overall accuracy was used to evaluate full CNNs, and F-scores to evaluate the performance of one CNN for different classes.

The overall accuracy is the ratio of true classifications over the total number of classifications. For multiclass classification, only true positives (TP) need to be considered, because a true positive for one class automatically corresponds to true negatives for the other classes. The total number of classifications is then equal to the sum of true positives and false negatives (FN).

$$\text{Overall accuracy} = \frac{TP}{TP + FN} \times 100\%$$

The F-score of a class  $i$  is computed by taking the harmonic mean of its precision and recall. Precision indicates how many positive classifications per class are actually true positives (as opposed to false positives, FP), whereas recall indicates how many true positives were positively classified. Because an F-score uses both these values, it is sensitive to both underestimation and overestimation (Kattenborn et al., 2021).

$$\text{Precision}_i = \frac{TP_i}{TP_i + FP_i}$$

$$\text{Recall}_i = \frac{TP_i}{TP_i + FN_i}$$

$$F_i = 2 \times \frac{\text{precision}_i \times \text{recall}_i}{\text{precision}_i + \text{recall}_i}$$

To my knowledge, there is no confidence interval associated with the F-score, and vegetation mapping studies do not tend to define acceptable lower limits of accuracy, precision, recall or F-score. At the minimum, the CNN should perform better than a ‘baseline model’ such as the ZeroR classifier, which predicts the most-frequent class (e.g. Osco et al., 2020; Wani et al., 2022). Additionally, in many studies the CNN performance is compared to the performance of a simpler model, such as RF or SVM, to ascertain that using a more complex model does in fact improve model performance (e.g. Barbosa et al., 2020; Guidici et al., 2017; Rezaee et al., 2018; Zhang et al., 2018).

### 3. METHODS

The methodology consisted of two main parts. First, a vegetation survey was conducted to study the coastal dune vegetation in the Bloemendaal blowout complex on the species level, and analyze the composition of different vegetation communities. Following the vegetation survey, a CNN was developed and trained to map coastal dune vegetation communities from high-resolution orthophotos, using aerial imagery from the Bloemendaal blowout complex. These two sections will be discussed separately, after a short introduction of the study site.

#### 3.1. Study site

This study was conducted in the Bloemendaal blowout complex, shown in Fig. 11 (52°25'35"N, 4°33'35"E). It is located in the Netherlands between Bloemendaal and IJmuiden between the regional RijksStrandpalen beach poles indicating 59.25 and 60.25 km (see Fig. 1). The study site stretches ca. 950 m along the North Sea coast, from the coastline to 550 m inland. It covers the beach, foredune (ca. 20 m in height) with trough blowouts, and part of the grey dunes beyond the foredunes. The dunes in this region are young and contain high concentrations of  $\text{CaCO}_3$  (Eisma, 1968). The study site is part of National Park Kennemerland-Zuid (NPKZ), which is managed by drinkwater company PWN. Since 2004, it is also a Natura 2000-area.

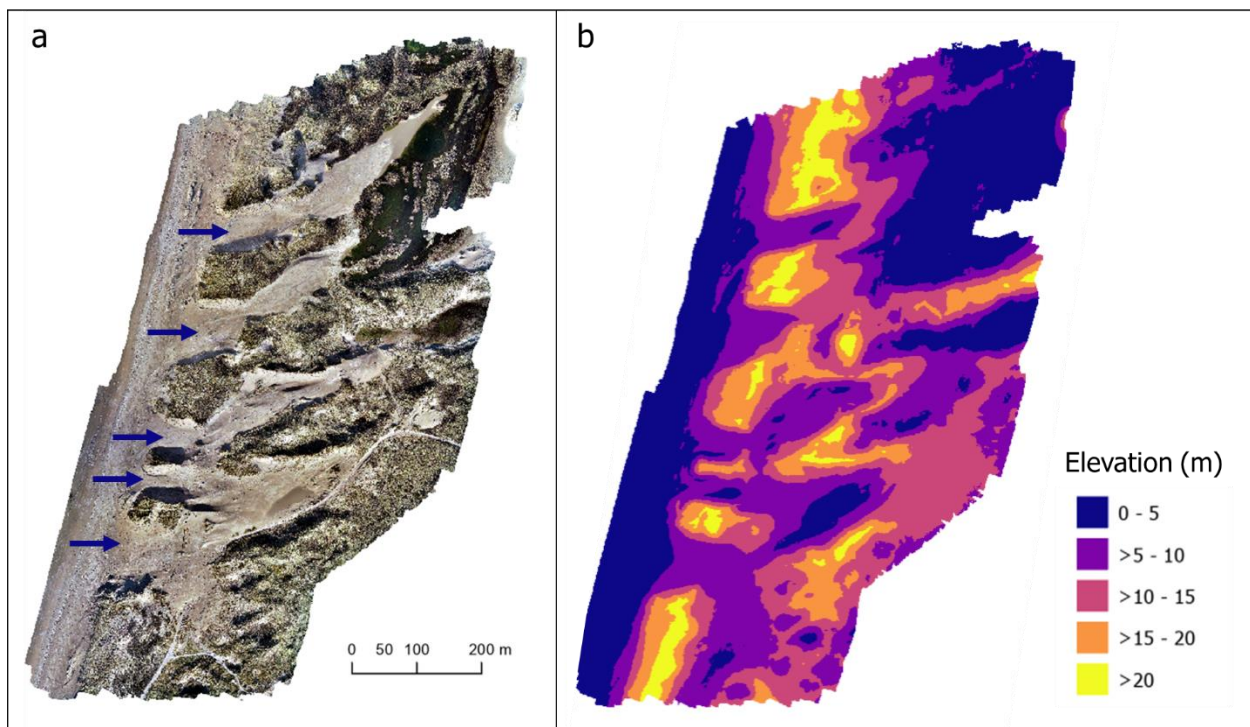


Figure 11: Orthophoto (a) and elevation map (b) of the study site. In (a), the five notches in the foredune of the blowout complex are indicated with blue arrows. The scale of (a) and (b) is the same. The orthophoto was assembled from the March 2<sup>nd</sup> 2022 UAV survey, the elevation map shows the DEM generated from this survey.

The blowout complex in the study site was created to return sand dynamics beyond the foredune. It is part of the Noordwest Natuurkern project, a collaboration of PWN, Natuurmonumenten and Hoogheemraadschap van Rijnland. In the winter of 2012 - 2013, five troughs were dug in the foredune, 100 to 150 m wide and ca. 12 m deep. In total, 120,000 m<sup>3</sup> of sand were removed (Kuipers et al., 2016). Over the years, the blowout complex has evolved considerably. The alongshore profile of the notches changed from V- to U-shaped troughs (visible in Fig. 3). The notches deepened as well, although they are still above the limit for coastal safety of 6 m above mean sea level (Ruessink et al., 2018).

Before the blowout complex was excavated, the site consisted of one continuous, dike-like foredune covered with marram, and a hinterland with open dune grassland (grey dunes and dune slacks), grass-encroached areas and buckthorn thickets (Everts et al., 2005). Like many Dutch coastal dune areas, NPKZ is negatively affected by excessive nitrogen deposition and subsequent grass encroachment and loss of biodiversity. Besides the creation of the blowout complex, PWN has introduced Scottish Highland cows, Konik and Shetland Ponies to the landscape to increase grazing pressure. NPKZ also houses rabbits, roe deer (*Capreolus capreolus*) and fallow deer (*Dama dama*) (Valdés-Correcher et al., 2018).

## 3.2. Vegetation survey

### 3.2.1. Fieldwork

A vegetation survey was performed to determine the vegetation composition in the study area and prepare for the visual identification of vegetation on aerial photos. 56 points were selected with a random stratified sampling method (Parsons, 2017), using Normalized Difference Vegetation Index (NDVI) data from the Copernicus Sentinel-2 satellites. 4 strata were used to cover the successional stages from bare sand to fully vegetated. In total, 4 bare sand points were selected, 8 sand/early pioneer vegetation points, 20 pioneer vegetation points and 24 fully vegetated points, to account for increasing species diversity in later successional stages. The points were obtained in ArcGIS Pro (Esri, USA) by reclassifying the NDVI map into 4 strata, transforming the resulting map into polygons and computing the number of samples per strata per polygon using this formula:

$$\text{Points per polygon} = \frac{\text{polygon area}}{\text{total strata area}} \times \text{total points per strata}$$

The random points were then created using the 'Create Random Points' function in ArcGIS.

Between February 22<sup>nd</sup> and March 7<sup>th</sup> in 2022, 44 of the selected points were surveyed (Fig. 12). The other points could not be accessed in time before bird nesting season started and access to the study site became restricted. At each point, a plot of 4 by 4 meter was set out. The exact location of the plots was measured with a differential global positioning system (DGPS). In the plots, the coverage of each plant species present was recorded. A vegetation expert assisted with identifying the dune flora. Scientific vegetation nomenclature followed *Heukels' Flora van Nederland* 24<sup>th</sup> edition (Duistermaat, 2020) for vascular plants, and *De Nederlandse Bladmossen* (Touw & Rubers, 1989) for mosses. Due to difficulties differentiating between species of small grasses (<10 cm in height), they were excluded from the data analysis entirely. In June, a return trip to the site was made to assess seasonal changes and confirm shrub identities (which had no leaves during the vegetation survey).

### 3.2.2. Statistical analysis

Statistical analysis of the vegetation data was performed to differentiate between the different coastal dune vegetation communities. All analyses were done in an R environment (version 4.0.0, R Core Team (2020)), using the packages *vegan* (Oksanen et al., 2022) and *isopam* (Schmidtlein et al., 2010).

First, the plots were clustered into vegetation classes based on plant occurrence and coverage using the Isopam classification algorithm (Schmidtlein et al., 2010, *isopam* function *isopam*), excluding plants occurring in one plot only and plots without vegetation. The classes were named based on their characteristic species and correspondence to known vegetation classes from literature.

Furthermore, total observation cover and observed species richness (including all observed plants) per plot were computed for each vegetation class. Additionally, elevation, measured with the DGPS (3-4 cm error in z-direction), was used to determine plot elevations for each vegetation class. Finally, non-metric multidimensional scaling (NMDS) with Bray-Curtis dissimilarity coefficients was performed on the plots and plant species, using *vegan's* function *metaMDS*, to assess the variation between the classes.

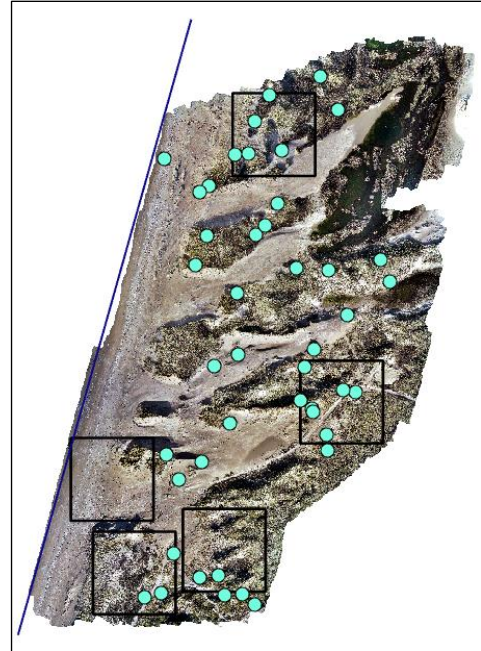


Figure 12: Locations of the plots (cyan points), the areas for which vegetation maps were generated (black squares) and the coastline defined to compute the plots' distances from the coastline (blue line).

### 3.3. Developing the vegetation-mapping CNN

The development of a CNN able to map vegetation from aerial imagery was divided in seven steps, as described in this section. First, a UAV survey was conducted to obtain orthoimagery and elevation data of the study site. Next, reference data for the CNN training was obtained by manually mapping the vegetation in part of the orthophoto. Using this reference data, the training and evaluation datasets were generated. Next, the CNN architecture with chosen hyper-parameters was initiated. Next, several CNNs were trained and then evaluated, given the research questions, using the orthoimagery, elevation data and reference data obtained previously. Finally, a vegetation map of the full study site was generated using the best-performing CNN.

#### 3.3.1. UAV survey

On March 2<sup>nd</sup>, 2022, a UAV survey was conducted to collect aerial imagery of the study site. Using a DJI Phantom 4 RTK UAV, 2481 images were collected. During the survey, the UAV kept a constant flight height between 55 and 65 m above mean sea level, without following the terrain.

To generate an orthophoto and a Digital Elevation Model (DEM) from the UAV images, a workflow presented by Over et al. (2021) was followed. This workflow was specifically developed for processing coastal UAV imagery with Structure from Motion analysis in Agisoft Metashape Professional Edition (version 1.6), the software used. First, a 3-dimensional point cloud was generated from the aerial imagery. The point cloud was then georeferenced using 10 Ground Control Points (GCPs, see Fig. 13), whose locations were measured with a DGPS. This resulted in root mean square errors (RMSE) of respectively 0.96 cm, 0.60 cm and 1.58 cm in the x, y and z-direction, yielding a total RMSE of 1.94 cm.

The orthophoto was generated with a resolution of 5 by 5 cm per pixel, high enough to recognize small-scale features such as individual tussocks of grasses, branches and footsteps in the sand. This made it possible to visually identify different types of vegetation. The DEM, generated to provide additional terrain information to the CNN, had a resolution of 1 by 1 m per pixel. The DEM was not corrected for vegetation heights.

### **3.3.2. Reference data generation**

Reference data to train the CNN with was generated by manually classifying and mapping the vegetation in the March 2<sup>nd</sup> orthophoto of the study site using ArcGIS Pro. The area of the vegetation maps was limited to five squares of 150 by 150 m, shown in Fig. 12, for a total mapped area of 112,500 m<sup>2</sup>.













In reference to the classes previously distinguished in the vegetation survey analysis, five classes were defined: 'sand', 'marram', 'buckthorn', 'grey dune' and 'privet'. All classes were well-recognizable in the orthophoto. Anything not belonging to one of these classes, such as dune slacks and man-made objects, was grouped in a sixth category, 'other'. A description of all classes with visual examples can be found in Table 1.

To make the vegetation maps, the vegetation belonging to each class was marked with polygons. The classification was based on visual identification, aided by brightness adjustments of the orthomosaic for the most shaded areas. Since each pixel can only belong to one class for the CNN to work, any overlap between polygons was removed. Finally, the polygons were transformed into a raster map where each pixel was classified.



**Figure 13: A GCP (black and white square) visible in the final orthophoto, together with the UAV operators. The real dimensions of the GCP are 50 by 50 cm.**

**Table 1: The vegetation classes distinguished in the vegetation maps. All examples are cutouts of 10 by 10 m in the orthophoto. Note that the specific class may not cover the entire image.**

Class	Description	Examples	
<b>Sand</b>	Bare sand without vegetation. Can contain shell/rubble fragments.		
<b>Marram</b>	<i>Calamagrostis arenaria</i> -covered area. Includes areas where bare sand is visible in between tussocks, excludes marram present in grey dune vegetation.		
<b>Buckthorn</b>	<i>Hippophae rhamnoides</i> -covered area.		
<b>Grey dune</b>	Grey dune vegetation, recognizable by high moss coverage. Typically individual plants were too small to be distinguished. In some places, marram tussocks were present.		
<b>Privet</b>	Wild privet ( <i>Ligustrum vulgare</i> ) shrubs.		
<b>Other</b>	All other terrain. Both other vegetation types and man-made objects. The example on the left contains a dune slack in the bottom half.		

### 3.3.3. Preparation of the CNN training and evaluation dataset

Preparation of the CNN training dataset, training and evaluation of the models and subsequent data analysis was done in an R environment (version 4.0.0, R Core Team (2020)) with the Keras API (Allaire & Chollet, 2022) and TensorFlow backend (Allaire & Tang, 2022). To work with the geospatial data, the R packages *sf* (Pebesma, 2018), *meteo* (Kilibarda et al., 2015) and *raster* (Hijmans, 2022) were used. R scripts of the code will be made available alongside this thesis.

To train and evaluate the CNN models, datasets including both input data (orthophoto and DEM) and desired

output data (vegetation map) were prepared. For these datasets, the data had to be divided into smaller tiles, to avoid exceeding available computer memory space. To test the effect of tile size on CNN performance, two datasets were assembled, one with tiles covering 5 by 5 m of the study site, and one with tiles covering 10 by 10 m. It was expected that increasing the tile size would give the CNN more context and improve its accuracy.

To make the datasets, first the orthophoto, vegetation maps and DEM were imported in R. The DEM was rescaled so that its values ranged from 0 to 255. Next, the orthophoto, vegetation maps and DEM were cropped into tiles using *meteo*'s tiling function. This yielded 4500 tiles of 5 by 5 m, and 1125 tiles of 10 by 10 m. The tiles were stored as .jpg images (orthophoto) or .png images (vegetation maps and DEM) of 200 by 200 pixels. The vegetation map tiles were stored as six separate images, one for each class. In each image, pixels were either black (0, class absent) or white (1, class present), as shown in Fig. 14. The separation of the classes in different images facilitated the division of one class per channel further in the preparation process ('one-hot encoding').

### 3.3.4. The CNN architecture and hyperparameters

For the CNNs, the U-net architecture (Ronneberger et al., 2015) was implemented using the *unet* function in the *unet* package. The U-net architecture has a characteristic U-shape and returns output with the same spatial dimensions as the input, so that each pixel is classified individually. The full architecture is shown in Fig. 8 and further discussed in the Theory, Section 2.3. The CNNs' input is either 3 channels (RGB) or 4 channels (RGB and DEM). Their output is 6 channels, one per class.

The hyper-parameters of the model are listed in Table 2. As output activation function, the softmax function was chosen. This function transforms the output so that each value is scaled to range between 0 to 1, such that the sum of values of all channels (representing classes) is 1 for each pixel. Therefore, the values can be interpreted as probabilities of the pixel belonging to each class. As loss function, categorical cross-entropy was chosen, which is very suitable for the multi-class classification of the CNNs in this thesis (e.g. Chen et al., 2020). Finally, the Adam optimization algorithm (Kingma & Lei Ba, 2015) was selected as optimizer because it has low memory requirements and high computational efficiency, and because it is well-suited for large datasets.

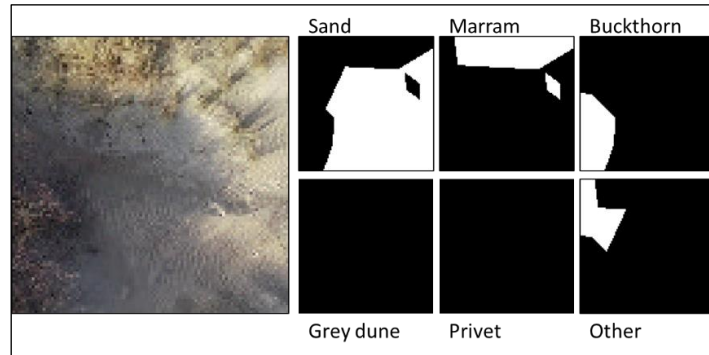


Figure 14: Example of one-hot encoding of a vegetation map tile (left): each class has its own image (right) with black or white pixels. When the six images are decoded and merged into one tensor with six channels, each pixel will contain one 1 value, and five 0 values.



**Table 2: Hyper-parameters of the CNNs.**

Hyper-parameter	Value
Input channels	3 (RGB) or 4 (RGB-DEM)
Activation function	Softmax
Optimizer	Adam
Loss function	Categorical cross-entropy
Batch size	8 (5x5) or 1 (10x10)
Number of epochs	15 (5x5) or 50 (10x10)

### 3.3.5. Training the CNNs

With the reference datasets and the untrained CNNs, the CNNs were trained. In the training workflow (Fig. 15), the full datasets were first split in evaluation and training datasets, containing respectively one and two thirds of the tiles. For the 5 by 5 m tile dataset, this resulted in 1500 evaluation tiles and 3000 training tiles, for the 10 by 10 m tile dataset respectively 375 and 750 tiles. The evaluation tiles were not used in the training process.

For each training session, the tiles used for training were split at random in a training and testing set, respectively containing 80% and 20% of the tiles. This was done with the `initial_split` function in the `rsample` package (Silge et al., 2021). To ensure that the CNN could ‘read’ the data, the image tiles were converted to tensors, one for input (with 3 or 4 channels for RGB and DEM) and one for output (with a channel per class, 6 in total). To keep the spatial resolution the same, the 5 by 5 m tiles were resized to 128 by 128 pixels, and the 10 by 10 m tiles to 256 by 256 pixels. To prevent the emergence of grey pixels in the vegetation map tiles, the resizing was done using nearest neighbor interpolation. The tiles in the training set were shuffled and augmented by flipping them at random (50% chance of flipping) and rotating them randomly in increments of 90 degrees. This was done to prevent the CNN from ‘learning’ to classify the vegetation based on arbitrary patterns such as the direction of shadows.

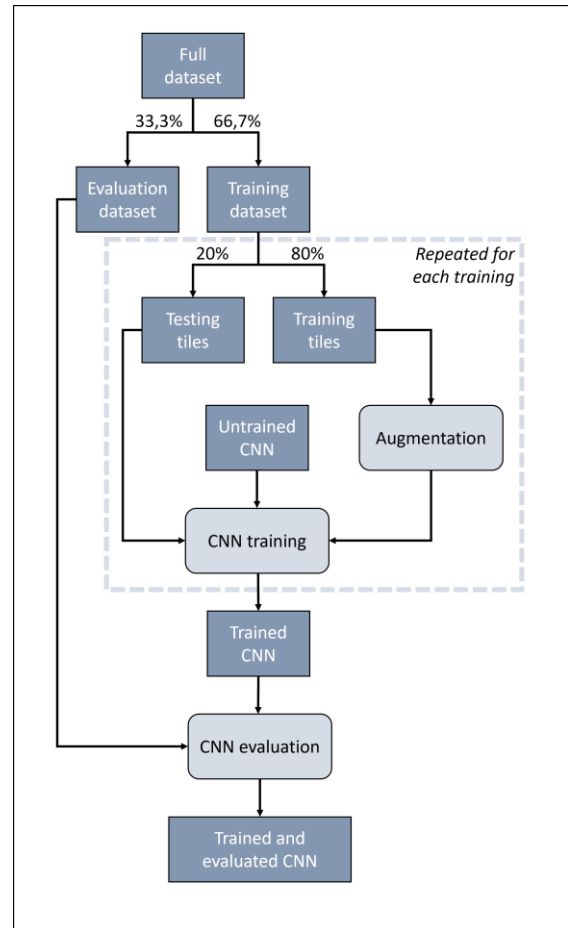


**Figure 15: Workflow to train and evaluate the CNNs. Processes are indicated with rounded rectangles.**

CNN types were named for their input tile dimensions (5x5 or 10x10) and whether their input included DEM (RGB or RGB-DEM). In total, four different types of CNNs were trained: 5x5 RGB, 5x5 RGB-DEM, 10x10 RGB and 10x10 RGB-DEM. For each type, 5 CNNs were trained to assess the effect of chance (in splitting, shuffling and augmentation of the dataset) on the CNNs’ final accuracy.

The actual training was performed on a computer with a CUDA-compatible NVIDIA GPU (NVIDIA GeForce RTX 3060). The batch sizes (how many tiles the CNN is presented with at a time) and epochs (how many times the full training set is repeated) were chosen to obtain optimal accuracy within the limits of available memory. These considerations are also discussed in Section 2.4. For the 5x5 CNNs it was possible to have a batch size of 8. These CNNs were trained for 15 epochs, when the accuracy of the test dataset stopped increasing. Due to memory restrictions, the 10x10 CNNs were trained in batch sizes of 1. These took longer to reach their optimum test accuracy in training, and were therefore trained for 50 epochs.

### **3.3.6. Evaluating the CNNs**

The models were evaluated with the evaluation tiles not used in training. To compare the 20 trained CNNs, overall accuracy was used as performance metric (Section 2.5). Performance differences between model types were analyzed using a Welch two-sample t-test, with differences being considered significant if  $p < 0.05$ .

The CNN with the highest overall accuracy was analyzed further to assess its accuracy per class. To do so, the CNN was used to classify each pixel in each tile in the evaluation dataset, counting the true positives, false positives and false negatives per class, as well as the total numbers of pixels per class in the reference data. From these values, the F-score and overestimation per class were computed. Furthermore, a confusion matrix was computed by counting all predicted classifications for each true class (from the reference data). Lastly, to understand the spatial patterns of misclassifications better, a misclassification heatmap was generated by summing the misclassifications per pixel of all the evaluation tiles.

### **3.3.7. Using the CNN to make vegetation maps**

In the final step, the CNN with the highest overall accuracy, one of the 10x10 RGB CNNs, was used to classify the vegetation of the entire study site. To do so, the orthophoto was divided into 5 sections in ArcGIS, to prevent overloading the computer's memory. The orthophoto sections were then imported into R. Each section was divided into tiles of 10 by 10 m, using *meteo's* tiling function, which were converted into tensors with 3 channels (RGB) and 256 by 256 pixels for the CNN. The preprocessed tiles were used as input for the CNN, which returned a classified tile, with one channel per class. For each channel/class, the classified tile was converted into a raster with geospatial data (from the original tile), using *raster's* raster and setExtent functions.

Finally, all raster tiles for the same class were merged, for all 5 sections, using *raster's* merge function. This resulted in 6 maps of the study area, one for each class, showing the probability of a class being present for each pixel. These 6 maps were exported into ArcGIS. In ArcGIS, a vegetation map was constructed, with pixels classified as the class with the highest probability for that pixel. Additionally, a probability map was constructed, showing the highest probability per pixel as measure of the CNN's confidence in its classification.

## 4. RESULTS

### 4.1. Vegetation survey

Between February 22<sup>nd</sup> and March 7<sup>th</sup> 2022, 44 plots in the Bloemendaal blowout complex were surveyed to analyze the ecosystem's vegetation composition. Five of the plots were bare, without any vegetation, and were therefore excluded from the vegetation analysis. In the other 39 plots, a total of 34 plant species were observed (excluding short grasses, <10 cm). Most frequently observed were *Calamagrostis arenaria* (marram, in 30 plots), *Hippophae rhamnoides* (sea buckthorn, in 25 plots) and *Rubus caesius* (European dewberry, in 19 plots). The full list of observed species and their occurrence frequencies can be found in Appendix A.

Clustering of the vegetated plots using the Isopam classification algorithm yielded four distinct vegetation classes. Examples of these classes, as well as bare sand, are shown in Fig. 16. The classes are characterized as follows:

- **Marram-dominated vegetation (14 plots):** This class was characterized by high marram cover, which was present in each plot. Other species occurring frequently were *Rubus caesius* and to a lesser extent *Hippophae rhamnoides*.
- **Buckthorn-dominated vegetation (11 plots):** Characteristic species for this class were *Hippophae rhamnoides*, which was present in all plots, and the tall grass *Calamagrostis epigejos*.
- **Grey dune vegetation (8 plots):** This class had a high number of characteristic species: mosses (*Hypnum cupressiforme*, *Syntrichia ruralis* and *Tortella flavovirens*), a fern (*Polypodium vulgare*) and several herbs (*Jacobaea vulgaris*, *Cerastium semidecandrum*, *Geranium molle*, *Erodium cicutarium*, *Cardamine hirsuta*, *Myosotis ramosissima*, *Saxifraga tridactylites* and *Fragaria vesca*).
- **Transition/other vegetation (6 plots):** The last class, named 'transition/other vegetation', included both grass-encroached plots (with as characteristic species *Carex arenaria*) and plots on a border or gradient between grey dune or marram-dominated vegetation and buckthorn-dominated vegetation.

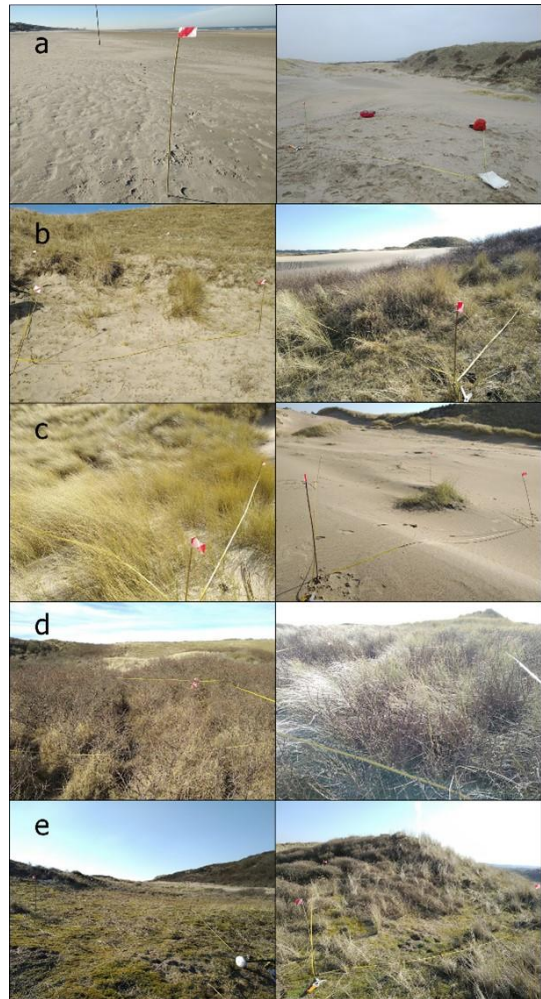


Figure 16: Examples of plots with the vegetation classes assigned by the Isopam algorithm. (a) bare sand (excluded from vegetation analysis), (b) transition/other vegetation, (c) marram-dominated vegetation, (d) buckthorn-dominated vegetation, (e) grey dune vegetation. Photographs taken during the vegetation survey in February-March 2022.

Other characteristic species were *Rubus caesius*, present in all 6 plots, and *Viola tricolor*, present in 2 plots.

The different classes showed clear differences in vegetation cover (Fig. 17a) and observed species richness (Fig. 17b) per plot. The transition/other class has a wide range in both observed species richness (median of 6.5) and vegetation cover (median of 65%). The marram-dominated class has the lowest observed species richness, with a median of 3, and together with the transition/other class the lowest vegetation cover (median of 65%) as well. The marram-dominated class also covers plots containing embryonal dunes, which could be one of the causes for the relatively low vegetation cover and species richness. The buckthorn-dominated class had a higher median vegetation cover (80%) and observed species richness (4) than the marram-dominated class, although for both these classes variation between plots was high. The grey dune class, lastly, has a median species richness of 13, indicating its biodiversity is far higher than for the other classes. It also has a median vegetation cover of 92.5%, very dense compared to the other classes. Both cover and species richness have a much narrower range as well, indicating stronger delineated boundaries of this vegetation class.

Comparison of plot elevation for bare sand and the different vegetation classes (Fig. 17c) shows strong variation and large overlap between the classes, indicating that they occupy the same elevation range. Overall, sand plots had the lowest elevation (median of 11.3 m, mean of 9.2 m), and buckthorn plots the highest (median of 14.7 m, mean of 13.4 m). All elevations were measured from ground height, so vegetation height is excluded from the total elevation.

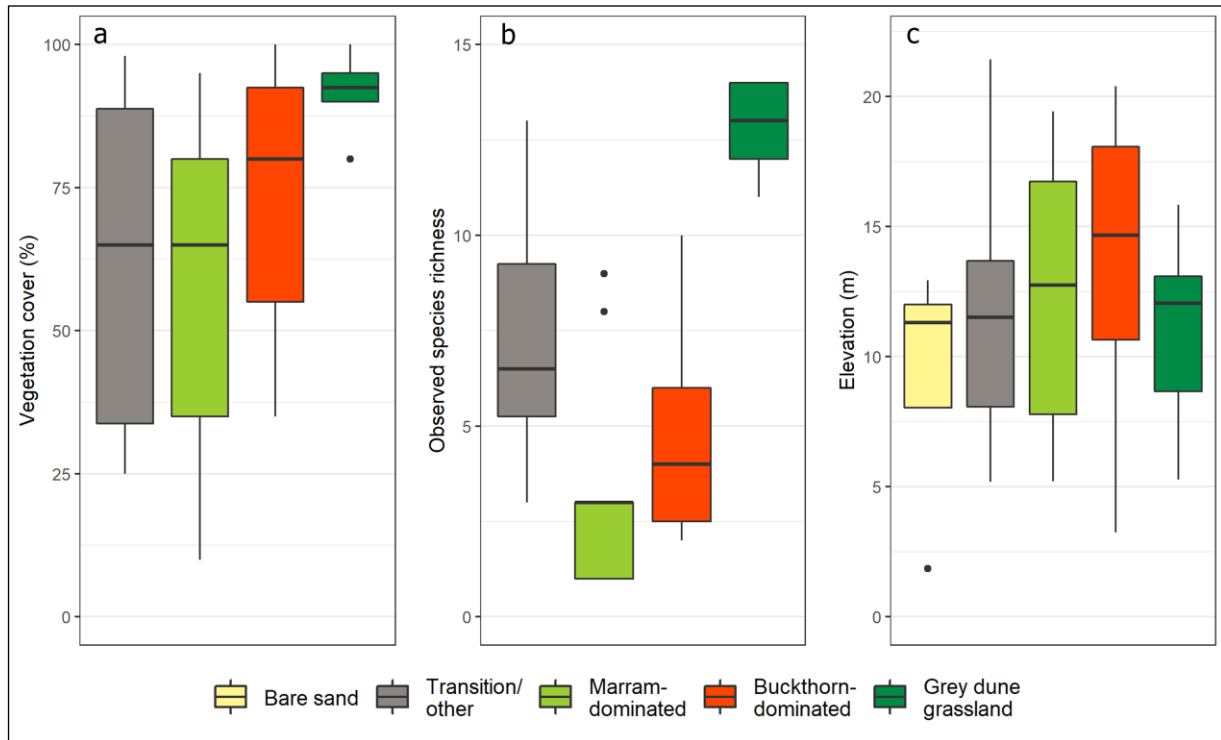


Figure 17: Boxplots of vegetation cover (a), observed species richness (b) and elevation (c) per plot during the vegetation survey in February-March 2022, grouped by vegetation class as assigned by the Isopam clustering algorithm. Small grasses (<10 cm) were included in the vegetation cover estimations, but excluded from the observed species count. Elevation was derived from the March 2<sup>nd</sup> DEM.

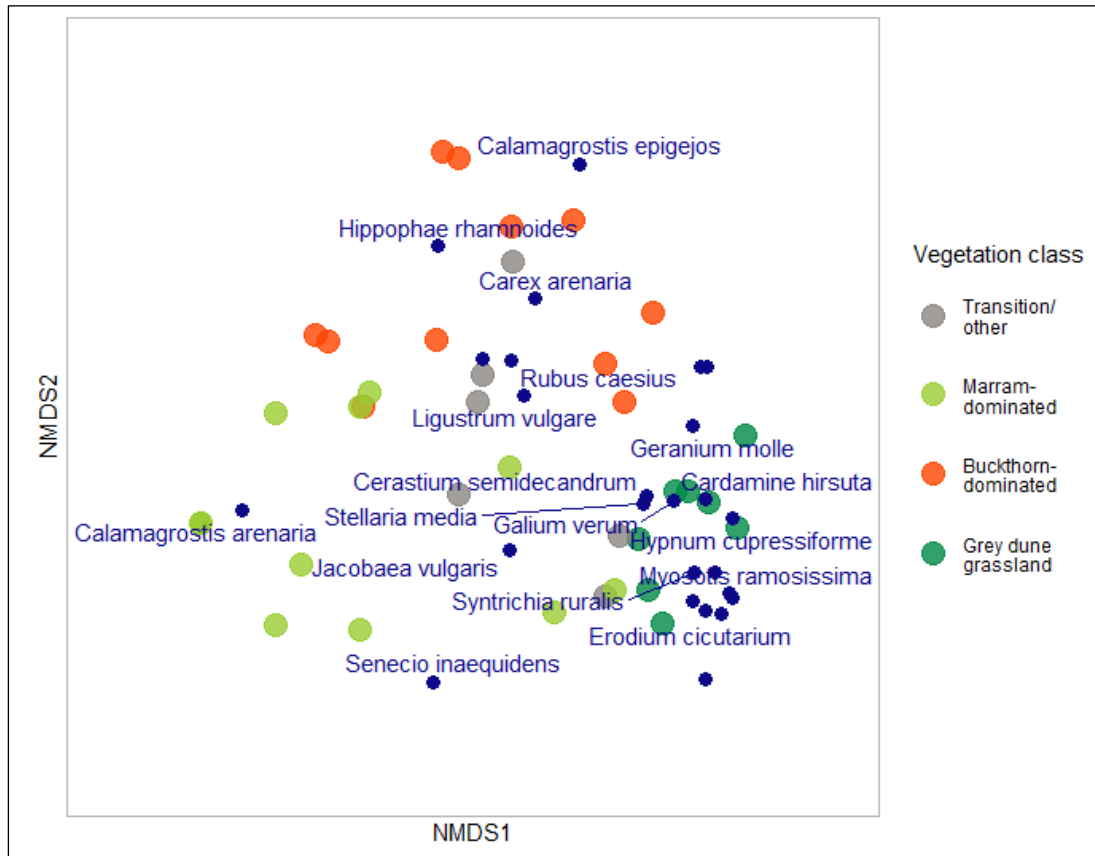


Figure 18: NMDS of the plots surveyed in the vegetation survey (colored by vegetation class as assigned by the Isopam algorithm) and observed species (dark blue points). Points that are closer together in the plot co-occur more often in the survey. For reading clarity, names of species occurring in less than five plots are not shown in the plot.

To study the variation between and within the vegetation classes further, a NMDS computation of the plots and species was performed. The resulting NMDS (Fig. 18) shows the plots arranged in a triangular pattern, with plots of marram-dominated vegetation, buckthorn-dominated vegetation and grey dune vegetation each occupying one corner of the triangle. The plots of the class previously dubbed ‘Transition/other vegetation’ are, indeed, in the center of the triangle, in between the other three classes.

One notable aspect of the NMDS plot distribution is the lack of clear boundaries between classes: some plots assigned to different classes were similar enough to overlap. Although the grey dune plots are grouped close together, indicating relatively high homogeneity within this class, the other plots are more scattered. The NMDS also shows a gradient in species richness from left to right: on the left, *Calamagrostis arenaria* is the only species present, in line with the low species richness observed in the marram-dominated plots. On the right the density of species is high, with a clear cluster of grey dune-specific species including mosses and small herbs. In the top of the NMDS, where the buckthorn-dominated plots are located, *Hippophae rhamnoides* is clustered together with the tall grasses *Carex arenaria* (sand sedge) and *Calamagrostis epigejos* (wood small-reed). *Rubus caesius* (European dewberry) and *Ligustrum vulgare*

(wild privet) are located in the middle of the triangle, in the transition space, suggesting they are not strongly bound to one specific class.

#### 4.2. CNN performance for different input data types

The 20 CNNs that were trained all achieved overall accuracies within a range of 67-76%. The highest overall accuracy was 75.8%, achieved by one of the 10x10 RGB models. This model was selected for the CNN-based vegetation classification of the entire study site. Furthermore, for this model the performance was evaluated for each class separately as well. A summary of the overall accuracies for each CNN type is listed in Table 3.

The inclusion of additional elevation data as CNN input was not found to affect model performance. Although there were differences between the mean RGB and RGB-DEM overall accuracies, the difference was not significant for either the 5x5 tiles ( $p = 0.968$ ) or the 10x10 tiles ( $p = 0.122$ ). The results did seem to suggest that DEM inclusion lead to a lower variance of the models (i.e. a lower standard deviation), but this was not investigated further.

The tile size, however, did have a significant impact on model performance. The mean overall accuracy of the 10x10 RGB-DEM models was 4.3 percentage points higher than that of the 5x5 RGB-DEM models, a significant difference with  $p = 0.004$ . The difference in tile size for the RGB models was not significant ( $p = 0.093$ ).

**Table 3: Evaluation of CNN performance for each type of CNN. For all types, n = 5.**

CNN type	Mean accuracy (st. dev.) (%)	Maximum accuracy (%)
5x5, RGB	70.6 (2.27)	73.1
5x5, RGB-DEM	70.7 (1.72)	73.2
10x10, RGB	73.2 (2.04)	75.8
10x10, RGB-DEM	75.0 (0.47)	75.6

#### 4.3. Class-based and spatial patterns in CNN performance

As stated previously, the best-performing 10x10 RGB model was selected for further performance analysis and to map the vegetation of the full study site. For the CNN classes (see Table 1 for examples), the classes bare sand, marram-dominated vegetation, buckthorn-dominated vegetation and grey dune vegetation were adapted from the vegetation survey. The class 'privet' (*Ligustrum vulgare*) was added to distinguish privet and buckthorn shrubs (see Section 5.2.2 in the Discussion). Vegetation previously grouped in the vegetation class 'transition/other' was either split in the relevant classes when it was on a transition between two main vegetation classes, or grouped under 'other' if it was a different vegetation type (such as grass-encroached terrain).

The evaluation per class, summarized in Table 4, shows strong differences in performance between the six different classes. For sand, grey dune, marram and buckthorn, the model achieved F-scores between 0.74 and 0.90, showing that the model could recognize and distinguish them very well. Privet and other scored significantly lower, with F-scores of respectively 0.30 and 0.50. For most classes, the total surface area as classified by the CNN was in good agreement with the class's surface area in the reference data, with less than  $\pm 5\%$  overestimation (Table 4). The two exceptions were sand, with an overestimation of 7.5%, and privet, with an underestimation of 67.8%.

Table 4: Evaluation of the best-performing CNN per class.

Class	Area in reference data (%)	F-score	Overestimation (%)
Sand	33.1	0.90	+ 7.5
Marram	20.7	0.76	+ 3.2
Buckthorn	16.6	0.74	+ 0.7
Grey	10.5	0.79	- 1.5
Privet	4.3	0.30	- 67.8
Other	14.8	0.50	-3.2

The F-score of a class appears to be positively correlated with the class’s relative surface area in the reference data (Fig. 19,  $R^2 = 0.579$ ): sand has both the highest surface area and F-score, and conversely privet has both low surface area and F-score. Grey dune, however, achieved a higher F-score than would be expected from its relative surface area (10.5%) alone.

To further analyze the CNN’s misclassifications, a confusion matrix was computed (Fig. 20), showing the CNN’s classifications for each class. On the diagonal lie the true positive classification fractions, where the predicted class matches the true class. These true positive fractions are highest for sand (93%) and grey dune (78%), and lowest for privet (20%) and other (49%) – in line with the overall F-scores listed in Table 4.

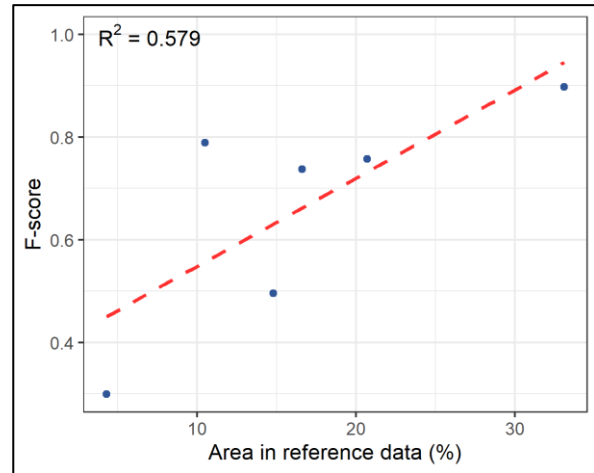


Figure 19: F-score per class as function of relative surface area.

Overall, the CNN performed worst for privet, which was only correctly identified for 20% of the true privet pixels. Privet was most often misclassified as buckthorn (28%) and ‘other’ (18%). Although privet had a high number of false negatives, there were barely any false positives, indicating a high precision: if the CNN classifies a pixel as privet, it probably is privet. Besides privet, the CNN appeared to have difficulties

True class	Predicted class					
	Sand	Marram	Buckthorn	Grey	Privet	Other
Sand	0.93	0.03	0.00	0.00	0.00	0.03
Marram	0.06	0.77	0.04	0.00	0.00	0.12
Buckthorn	0.02	0.08	0.74	0.03	0.02	0.11
Grey	0.00	0.02	0.06	0.78	0.01	0.12
Privet	0.01	0.15	0.28	0.17	0.20	0.18
Other	0.22	0.16	0.08	0.05	0.01	0.49

Figure 20: Confusion matrix for the best-performing CNN, listing the fractions of CNN-predicted classes for each true class (based on the reference data). The colors (blue = low, red = high) were added for readability.

with the 'other' class, yielding high numbers of both false positives and false negatives. With exception of sand, for all other classes over 10% of the pixels was misclassified as 'other'. On the other hand, pixels of class 'other' were often misclassified as sand (22%) or marram (16%).

Finally, to gain a better understanding of how the errors were distributed spatially on the input tiles, a heatmap was generated of the distribution of misclassified pixels. For this, the full evaluation dataset was used, containing 375 tiles of 10 by 10 m (256 by 256 pixels). The highest number of misclassifications per pixel was 129 (34.4% of the total classifications), the lowest number 63 (16.8%). The misclassification heatmap (Fig. 21) is quite uneven, indicating that the randomness of spatial patterns in the input tile contents is a significant factor in the misclassification heatmap. However, in the heatmap it is clear that misclassifications occur more often close to the edges and particularly the corners of the tiles. Additionally, there is also a 'hotspot' just south of the tile center.

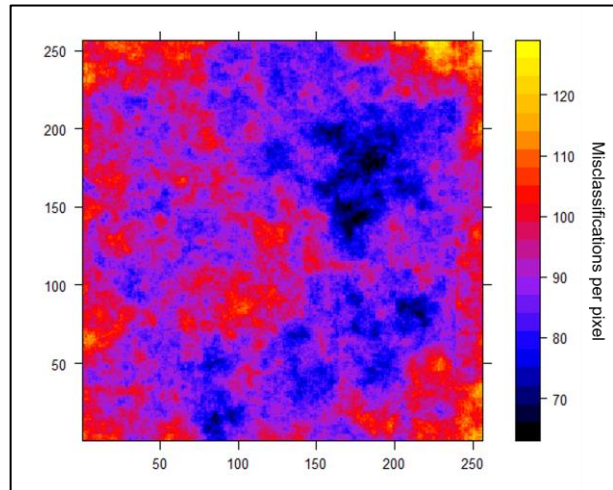


**Figure 21: Spatial distribution of misclassifications in the 375 evaluation data tiles. The tiles are 256 by 256 pixels and represent 10 by 10 m.**

#### **4.4. CCN-based vegetation classification of the full study area**

Using the best-performing CNN, a vegetation map of the full study area was generated based on the March 2<sup>nd</sup> 2022 orthophoto (Fig. 22a and b). The full-size version of this map is included as attachment to this thesis, because of its large size (A2, scale 1:2,000).

The vegetation map (Fig. 22b) clearly shows the beach (bare sand) and marram-covered foredune ridge, interspersed by the five blowouts. The blowouts' depositional lobes, angled towards the northeast, reach lengths of over 400 m landwards. The vegetation bordering the depositional lobes mainly consists of marram. Further away from the bare sand, marram is succeeded by sea buckthorn shrubs and grey dune grassland. The vegetation here appears varied, with small-scale patches of buckthorn, grey dune, privet and 'other' vegetation.

The dominant vegetation classes (excluding bare sand) in the Bloemendaal blowout complex are marram, buckthorn and grey dune. These three seem balanced, without one class clearly overpowering the others. There are also some privet thickets present in the blowout complex (see also the close-up in Fig. 23a), but they did not cover large areas and were not recognized well by the CNN (Fig. 23b). There are also some areas labeled as 'other' in the vegetation map (Fig. 22b), which could be other vegetation types (like dune slack vegetation or tall grass-encroached areas), misclassified marram, buckthorn, grey dune or privet, or something artificial such as the bicycle track in the south of the blowout complex. However, the 'other' surface area is quite low compared to the surface area of sand, marram, buckthorn and grey dune.



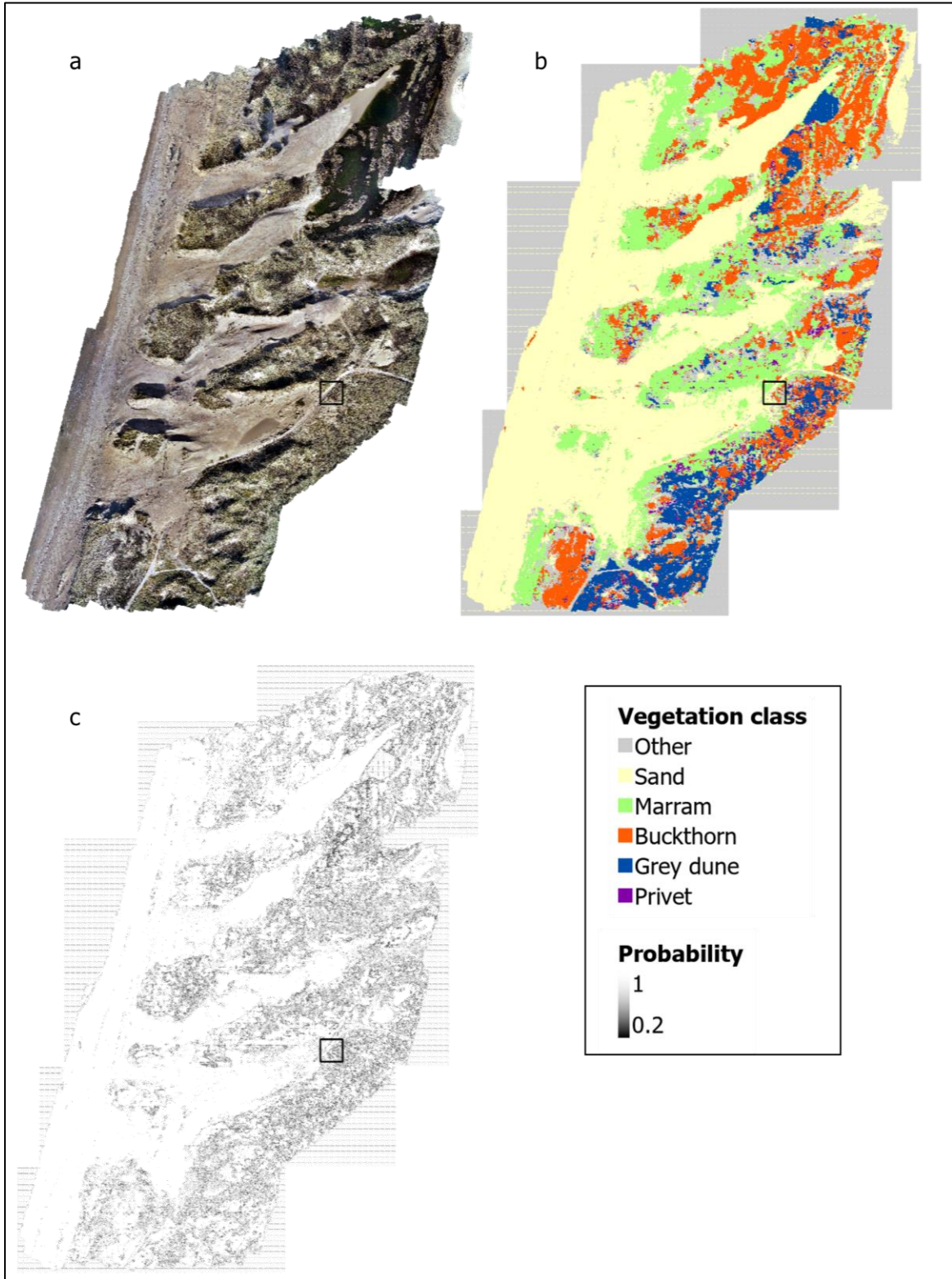


Figure 22: The March 2<sup>nd</sup> orthophoto (a), corresponding CNN-classified vegetation map (b) and classification probability map (c) of the Bloemendaal blowout complex. The black square in the maps indicates the location of the close-ups shown in Fig. 23.

One feature the CNN did not handle well is the water of the dune slacks in the northeast of the study site (Fig. 22a), which was not included in the CNN training dataset. The CNN classified the water areas primarily as either grey dune or buckthorn, whereas the correct classification would be 'other'. Furthermore, particularly in the regions with more varied vegetation further inlands, an edge effect has occurred: classification patterns clearly show the tile edges as borders between different classes (Fig. 23b).

Besides the vegetation map, a corresponding probability map was also generated (Fig. 22c). This map gives the probability of each pixel classification being true (according to the CNN) and gives an indication of the CNN's confidence. The probabilities per pixel ranged between 0.20 and 1, with a mean probability of 0.88. Generally, the bare sand on the beach and in the blowouts and deposition lobes had the highest probability, whereas in vegetated areas probabilities were lower (Fig. 22c). Zooming in, it appears that probabilities are lowest at boundaries between different classes, in particular in areas where different vegetation classes form small patches (Fig. 23c).

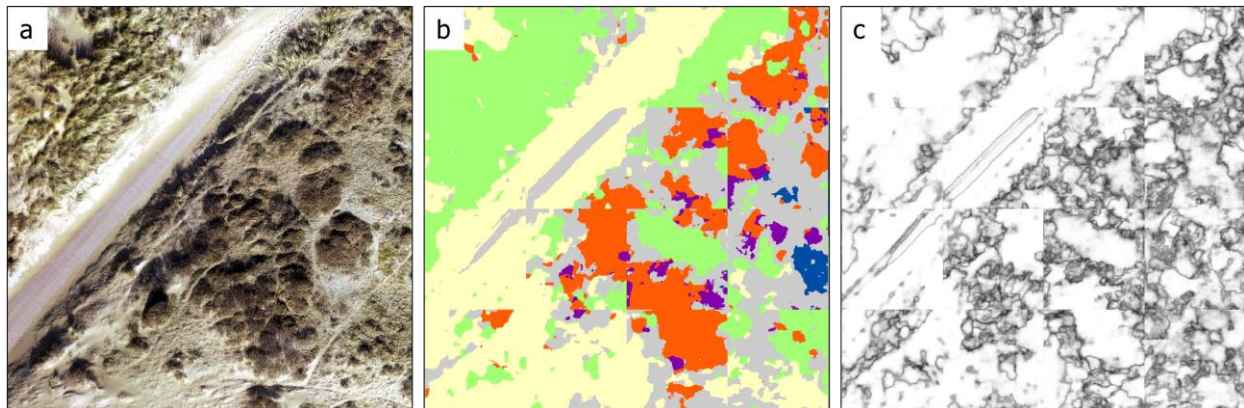


Figure 23: Close-up of the orthophoto (a), vegetation map (b) and probability map (c). The close-up is 40 by 40 m in size, and its location in the blowout complex is indicated in Fig. 22. The legends of the vegetation map and probability map are the same as in Fig. 22.

## 5. DISCUSSION

### 5.1. Mapping coastal dune vegetation with CNN

The results of this thesis show that using a CNN in combination with remote sensing data is a promising method for coastal dune vegetation mapping, achieving an overall classification accuracy of 75.8%. The best-performing CNN was a multiclass CNN trained on RGB input data with tile dimensions of 10 by 10 m. Although there are still a number of improvements that must be made before the CNN can be used in practice, this overall accuracy of 75.8% is already comparable to those achieved in vegetation mapping studies with similar use of remote sensing data and machine learning.

While there has not been much focus yet on coastal dune ecosystems in the field of CNN vegetation mapping, the CNN presented in this thesis can be compared to CNNs trained for other ecosystems. For example, Kattenborn et al. (2019) achieved accuracies between 84% and 90% for classification of species and communities in forests and glacial foreland. These significantly higher accuracies could in part be due to their study sites being less dynamic in terms of vegetation burial by sand, which complicated classification. Another possible factor is that they trained CNNs to detect one specific species or community, instead of classifying all vegetation types in the study area. This would make the classification task less complex, which could improve overall accuracy.

Compared to coastal dune vegetation mapping studies, the overall accuracy of 75.8% achieved in this thesis is comparable to the ones obtained by Suo et al. (2019), who used a maximum likelihood classification algorithm using either RGB or multispectral data and obtained overall accuracies of respectively 68.5% and 78.2%. Conversely, (Medina Machín et al., 2019) obtained a significantly higher overall accuracy of 88.03% with a Support Vector Machine using multispectral data and texture information. Potentially, improvements of the CNN (which will be discussed further below) could lead to accuracies approaching or even surpassing the ones obtained using multispectral data. This could be a very worthwhile endeavor, as it would eliminate the need for relatively inaccessible and expensive multispectral data to create vegetation maps from remote sensing data.

### 5.2. The coastal dune vegetation in the Bloemendaal blowout complex

#### 5.2.1. The main vegetation classes

The main vegetation classes found during the vegetation survey (Fig. 16) were marram-dominated vegetation, buckthorn-dominated vegetation and grey dunes. Additionally, some of the plots were unvegetated (bare sand), and some plots were grass-encroached or on a boundary between two of the main vegetation classes (transition/other vegetation). Within the main vegetation classes, biodiversity in vegetation (measured as observed species richness, Fig. 17b) increased from marram-dominated vegetation, with a species richness median of 3, via buckthorn-dominated vegetation to grey dunes, with a species richness median of 13.

The main vegetation classes found during the vegetation survey are comparable to the habitat types in the Natura 2000 framework for dry coastal dune ecosystems discussed in the Introduction (Section 1.1): marram-dominated vegetation with 'white dunes' (H2120), buckthorn-dominated vegetation with 'dunes with *Hippophae rhamnoides*' (H2160) and grey dune with 'grey dunes' (H2130). The similarity of the

vegetation survey classes and Natura 2000 habitats indicates that no important vegetation classes were missed during the survey.

Because of limited access to the study site during the bird nesting season, the vegetation survey was conducted in late February and early March, when most plants were not blooming yet. Nevertheless, with assistance from a dune vegetation specialist all but one plant species could be identified to the genus or species level, except for the small grasses. The unidentified small grasses mainly occurred in the grey dune vegetation, which could indicate that grey dune biodiversity was actually underestimated in the vegetation survey.

Additionally, the time of surveying could have influenced the observed species richness and coverage values. For example, the annual plants found during the vegetation survey were mainly winter annuals blooming in early spring, while summer annuals had not sprouted yet. Other, perennial plants, did not have leaves during the vegetation survey (e.g. *Rubus caesius*), which strongly limited their relative vegetation cover. However, even though exact species composition and characteristics might vary between seasons, the return visit in June and the literature on coastal dune ecology (as reviewed in Section 1.1) both indicate that the general vegetation class characteristics observed in the vegetation survey are reliable.

### **5.2.2. Translation from vegetation to CNN classes**

The main vegetation classes found in the vegetation survey could be effectively translated into classes for the CNN because they were well-distinguishable by eye on the high-resolution orthophoto of the blowout complex (see Table 1 for examples). Besides the classes sand, marram, buckthorn and grey dune, the classes 'privet' and 'other' were added as CNN classes. The shrub privet (*Ligustrum vulgare*) was chosen because, while it is a shrub just like buckthorn, it could potentially be interesting to distinguish between the two: buckthorn is a pioneer shrub associated with primary succession, whereas privet only establishes in areas with further soil development in later succession stages (Provoost & Declerck, 2020). Additionally, grazing patterns on privet and buckthorn differ (Valdés-Correcher et al., 2018), which could have implications on the introduction of grazers to the coastal dune landscape as measure against shrub encroachment. The class 'other' was added because for a multiclass CNN such as the one in this thesis, all pixels must be classified.

One difference between the vegetation classes in the vegetation survey and the CNN classes were their spatial boundaries: whereas in the survey multiple plots were found on a transition between two main vegetation classes (such as between buckthorn and grey dune vegetation), in the CNN reference data boundaries were often drawn at a higher resolution (the level of individual shrubs), removing these 'transition' vegetation types. Furthermore, grass-encroached (non-marram) areas were included in the class 'other'. Besides these differences, the CNN classes were very similar to the vegetation classes from the vegetation survey.

Additionally, the CNN classes can be translated into the habitat types in the Natura 2000 framework for dry coastal dune ecosystems. This is particularly relevant because it allows for comparison of the CNN's results with other studies, which also often use the Natura 2000 habitats. In the future, the CNN could be used for vegetation studies in Natura 2000 regions, for better ecological understanding and better nature management.

### 5.2.3. *The blowout complex' vegetation map and vegetation distribution*

In the CNN-generated vegetation map of the Bloemendaal blowout complex (Fig. 22b) a clear sea-inland successive gradient of the main vegetation classes can be seen, for example in the southernmost area. The beach, where conditions are too harsh for vegetation to grow, consists of bare sand. The foredune is covered with marram, a pioneer which thrives on sand burial. Further landward, marram is succeeded by buckthorn and then grey dunes. This succession in vegetation classes also indicates that the species richness increases along the sea-inland gradient, in line with a global trend in species richness in coastal dune ecosystems (Tordoni et al., 2021).

The clear successional gradient, with linear zonation of vegetation along the coastline, is strongly disrupted by the five blowouts. Their depositional lobes reach hundreds of meters inland, and bordering is pioneer vegetation – marram, one of the earliest successional stages. This implies that the creation of the artificial blowout complex was effective in 'resetting' the vegetation to earlier successional stages – also 9 years after creation. There is not one clearly dominant vegetation type, although there would presumably be far less marram present without the blowouts increasing sand dynamics inland of the foredune. Not much privet can be seen, assigned partially to the CNN's difficulties recognizing privet, and partially because these dunes are not old enough yet for a strong privet presence.

To analyze the effect of the blowout complex on the vegetation further more knowledge on the vegetation distribution before the excavation of the blowouts is required. For this, the 1:5,000 vegetation map of the Kennemer dunes published in Everts et al. (2005)<sup>2</sup> was compared to the 1:2,000 CNN-classified vegetation map. The 2005 map shows the continuous marram-covered foredune and backdunes that are almost entirely vegetated, with barely any patches of bare sand – rather different from the current situation. The vegetation in the backdunes in 2005 showed a patchwork of different vegetation types, just like the present-day and also reported by Doing in 1988. Generally, the vegetation classes were the same in both maps, although Everts et al. (2005) distinguished far more specific subclasses (>20 in the study site) and also included dune slack vegetation, which was not included in this thesis' vegetation classes since the vegetation close to dune slacks was not surveyed.

In 2005, the vegetation appeared to be dominated by buckthorn and other shrubbery like wild privet, European dewberry (*Rubus caesius*) and common hawthorn (*Crataegus monogyna*), and additionally some areas were fully encroached by tall grasses, such as sand sedge (*Carex arenaria*). Although there were some grey dune areas present in 2005, all grey dune area was classified as 'poorly developed'. Particularly in the southmost part of the study site, grey dune area has increased significantly from 2005 to 2022. This could indicate that the blowout complex is effective in promoting grey dune vegetation, a very promising sign considering the high ecological value and priority habitat status of grey dune grasslands (Council of the European Commission, 1992). However, more research must be conducted to separate the blowout complex' influence from that of other measures such as introduction of great grazers and manual buckthorn removal. Either way, this change shows that it is possible to recover grey dune areas in shrub- and grass-encroached coastal dune areas.

---

<sup>2</sup> A pdf of this report (in Dutch) can be accessed at [https://eco-on-site.nl/mirrors/pwn-puur-natuur/pdfs/vegetatiekartering\\_kennemerduinen\\_2005\\_everts\\_ea\\_2006.pdf](https://eco-on-site.nl/mirrors/pwn-puur-natuur/pdfs/vegetatiekartering_kennemerduinen_2005_everts_ea_2006.pdf). The vegetation map covering the study site is on page 135.

### 5.3. Effects of additional input data on CNN performance

#### 5.3.1. Elevation data as extra information

The overall accuracies of the 20 CNNs trained with or without additional elevation data (Table 3) do not show a significant improvement obtained by the inclusion of elevation data. This is in line with the elevation of the plots of different vegetation classes in the vegetation survey (Fig. 17c), which showed strong overlap between the classes. This indicates elevation would be unhelpful in distinguishing between them. Inclusion of elevation data in other CNN vegetation mapping studies have led to mixed results: Kattenborn et al. (2020) and Nezami et al. (2020) did not find significant improvements of elevation data on CNN performance, similar to the findings in this thesis. On the other hand, a study by Sothe et al. (2020) found that inclusion of elevation data significantly increased CNN performance.

A potential option to use elevation data for improved CNN performance would be to use elevation data with higher spatial resolution. The DEM used in this thesis was not corrected for vegetation height and had a resolution of 1 by 1 m per pixel. By increasing the resolution, to for example to the same resolution as the orthophoto (5 by 5 cm), the DEM could aid in recognizing borders of vegetation. For example, the edge of a buckthorn or privet shrub in a grey dune area could be recognized by the height difference of the two classes. If effective, this would be particularly useful because the CNN's confidence (measured as highest probability) was lowest at borders between classes (Fig. 23c).

#### 5.3.2. Alternatively: cross-shore distance data as extra information

An alternative type of additional CNN input data could be the distance from the coastline, or cross-shore distance. Since the coastal dune ecosystem is characterized by sea-land vegetation gradients and linear zonation, distance from coastline could be a better indicator of which vegetation is found on what location. To test this, an additional vegetation analysis was performed by computing distance from a pre-defined coastline (shown in Fig. 12) for each plot in ArcGIS, and processing this data in the same way as the elevation data (discussed in Section 3.2.2). The resulting boxplot is shown in Fig. 24. It shows that sand is generally closer to the coastline than the other classes and grey dune further, but also that there is a lot of overlap between transition/other, marram- and buckthorn-dominated vegetation. Since the classes sand and grey dune are already distinguished relatively well by the CNN (Table 4), it is unclear if additional cross-shore distance information would have made a significant difference on CNN performance.

However, the relationship between vegetation type and distance from coastline might be more pronounced in coastal dune systems with a continuous foredune, without blowouts that disrupt the linear vegetation zonation. This would require further study. If inclusion of distance from coastline did improve CNN performance in more linear dune systems, however, it might unintentionally create a bias

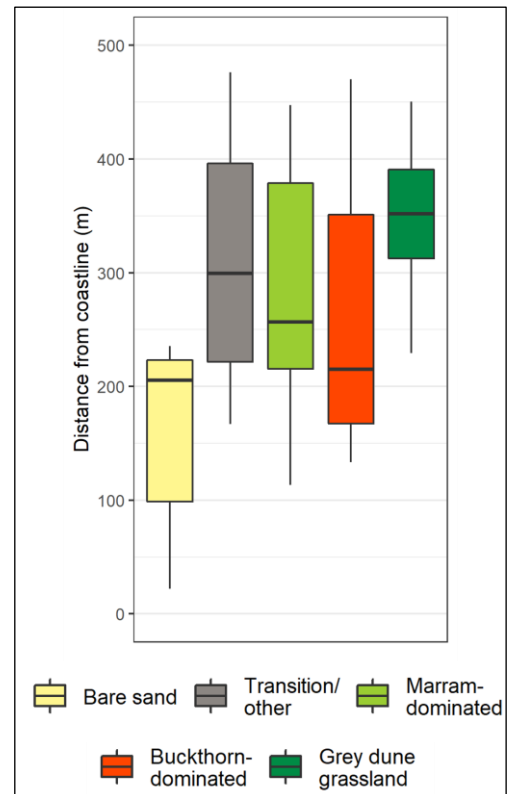


Figure 24: Boxplot of distance from coastline (cross-shore distance) per plot, grouped by vegetation class as assigned by the Isopam clustering algorithm.

against vegetation in the ‘wrong’ location, such as the marram meadows in the blowout complex that stretch out into the backdunes. Perhaps a better course of action would be to improve the CNN’s ability to classify vegetation based on RGB information only, so that additional information would not be required either way.

#### **5.4. Effects of input tile size on CNN performance**

Comparison of the performances of the CNNs using either 5 by 5 m or 10 by 10 m input tile size shows that doubling the input tile dimension significantly improves CNN performance (Table 3). This is in accordance with other studies by (Nevavuori et al., 2019) and (Kattenborn et al., 2020), which found that CNN performance significantly improved when increasing tile size respectively from 10 to 40 m and 2 to 5 m. The improvement at larger tile size could be due to the relatively smaller number of pixels located close to the tile edges and corners, which have less spatial ‘context’ provided by surrounded pixels. These pixels must be classified with less available information, and are therefore more prone to be misclassified (as seen in Fig. 21). This explanation implies that, if computer memory limitations would allow it, increasing the tile size further could improve the CNN’s performance even more.

The difficulties of classification edge and corner pixels relate to the edge effect visible in Fig. 23b, where the straight lines and right angles of the tile edges are visible. This effect is quite common in CNN mapping studies. To prevent it, an effective approach is to generate the vegetation map twice or thrice, with shifted origin positions, so that the tile borders of the multiple maps overlap. These overlapping maps can then be averaged to obtain an edge-less vegetation map (T. Kattenborn, personal communication, June 24, 2022).

#### **5.5. CNN performance per class**

##### **5.5.1. General remarks**

The analysis of performance (measured as F-score) per class showed that the CNN’s performance varied strongly for the different vegetation classes (Table 4). Sand and grey dune were recognized best, with F-scores of respectively 0.90 and 0.79, whereas privet and other were recognized worst, with F-scores of respectively 0.30 and 0.50. Overall, F-score was found to be positively related to total surface area in the reference dataset (Fig. 19). This can be explained by the fact that if the CNN is trained on more data from a certain class, it has more examples to learn how to recognize that class. Additionally, if the area fraction of a class is higher in the reference data, misclassification of that class will have a larger penalty during the training, so correctly classifying that class becomes more rewarding.

Besides the area in the reference data, the visual homogeneity of a class could also be a factor in how well the CNN recognizes it. Both grey dune and sand look relatively even, without much variation in patterns and colors, and particularly for grey dune (which covered 10.5% of the reference data) this could explain its relatively high F-score.

The best-performing CNN’s overall accuracy of 75.8%, which means that a quarter of its classifications were misclassifications. Considering the confusion matrix (Fig. 21), most errors appear to be related to the ‘other’ class and privet class, as well as vegetation classes that tend to border each other in the coastal dune ecosystem. The latter could partially have been due to the reference vegetation maps being constructed out of polygons, which approximated the real vegetation borders but did not exactly follow them.

### 5.5.2. *Privet*

As percentage, the class misclassified most often was privet, which was only correctly classified in 20% of the total classifications (Fig. 20). However, overall this did not have a great effect on the overall accuracy, since privet had a very low surface area (4.3%, Table 4). The low surface area can also explain why the CNN performed so poorly for this class. The confusion matrix showed that privet was most commonly misidentified as buckthorn (Fig. 20), presumably due to the visual similarity of the two shrubs.



Figure 25: Buckthorn thickets in February (left) and in June (right).

Besides including more privet in the reference data, a solution for the CNN's

poor performance for privet could be to merge the 'buckthorn' and 'privet' classes into a new class: 'thicket', which could decrease the CNN's specificity but potentially increase its overall accuracy.

Alternatively, the CNN might distinguish privet and buckthorn better if an orthophoto from a different season was used for training. In the March 2<sup>nd</sup> orthophoto used in this thesis, neither buckthorn nor privet carried any leaves. During the return visit to the study site in June, both shrubs looked very different (see Fig. 25 for buckthorn). More generally, the CNN could be trained on reference data from summer or autumn, to learn how to distinguish vegetation in different seasonal stadia. Potentially, one CNN could be trained for all seasons so that it could be applied any time of the year. This approach has proven to be successful before, for instance for the land cover classification set in the San Francisco Bay Area (USA) by Guidici et al. (2017).

### 5.5.3. *Other vegetation and terrain types*

The 'other' class was also challenging for the CNN. Correctly classified in 49% of the total classifications, this class was also associated with a large amount of false positives, e.g. other classes were misclassified as 'other'. Most misclassified 'other' pixels were classified as sand instead (22%), and to a lesser amount marram (16%). Confusion with sand can for example be seen in Fig. 23, where the bicycle road has for the most part been classified as sand. Additionally, three storms hit the Netherlands on February 16<sup>th</sup>, 18<sup>th</sup>, and 20<sup>th</sup> (named Dudley, Eunice and Franklin, see Mühr et al. (2022)), about two weeks before the UAV survey was conducted. This resulted in much vegetation, especially marram and buckthorn close to bare sand areas, being partially buried by sand. The resulting terrain was complicated to classify: not bare sand since the tips of marram blades were visible, but not convincingly marram either. Therefore, these areas were sometimes classified as 'other', but that might have caused confusion for the CNN.

Additionally, the 'other' class was a highly diverse catch-all of any area not belonging to the other five classes, including other vegetation, ambiguous terrain and human-built objects. Such heterogeneity might complicate the identification of features characteristic for this class. To improve the CNN's accuracy and increase its specificity, the 'other' class could be divided in multiple classes, such as 'artificial structures', 'grass-encroached area', 'buried vegetation' and 'dune slack vegetation'. This would require



more reference data to properly train the model, but could both increase overall accuracy and make the model more broadly applicable.

One terrain type that occurred in the orthophoto but not in the reference dataset was water (Fig. 22a, northeast). The CNN incorrectly classified this as either grey dune or buckthorn, which leads to an overestimation to the total surface area covered by these vegetation classes. Since dune slacks are a frequent feature in coastal dune ecosystems (e.g. Doing, 1995; Grootjans et al., 2004), it is essential to include water in the CNN's training process before it can be applied to a wider range of coastal dune regions.

## 5.6. Outlook

### 5.6.1. Combining CNN vegetation mapping with vegetation surveys in the field

While CNN can offer a very good addition to large-scale vegetation studies, field surveys remain indispensable for monitoring and understanding vegetation dynamics on the species level. Although different habitats are well-recognizable on high resolution orthophotos, by eye and by CNN, individual plants cannot typically be discerned. Therefore, a combination of CNN-based vegetation mapping and vegetation surveys can be used to monitor different vegetation types and their composition and biodiversity over time. Although including vegetation surveys is more time-consuming, it could have a number of benefits in understanding vegetation dynamics.

Firstly, single plants can easily be overlooked on large-scale orthophotos and resulting vegetation maps, even if their presence could give extra information on their local abiotic conditions. For instance, during the return visit to the study site in June 3<sup>rd</sup> 2022, the burial-dependent pioneer *Cakile maritima* was encountered at the back of one of the depositional lobes (Fig. 26). This plant typically lives seawards of the foredune (Davy et al., 2006), so its presence on the depositional lobe could indicate landward aeolian transport of *C. maritima* seeds via the blowout complex.

Additionally, with vegetation surveys abundance of invasive species that affect coastal dune dynamics can be monitored. For example, in the vegetation survey the invasive exote *Senecio inaequidens* was found in 20.5% of the vegetated plots. *S. inaequidens* is burial-tolerant and was found both in the grey dunes and white dunes. A recent study on interactions between *S. inaequidens* and marram by Van De Walle et al. (2022) found that *S. inaequidens* promotes marram growth, suggesting an increase in *S. inaequidens* could accelerate coastal dune succession. Understanding such dynamics on a small scale could help in understanding them on a large scale.

### 5.6.2. Potential further CNN applications

The field of CNN vegetation mapping is rather new and is developing fast. It offers great potential for ecological surveys – after the time-intensive reference data generation and CNN training phases, the actual mapping of the study site took just a few hours. While the CNN with the highest accuracy in this

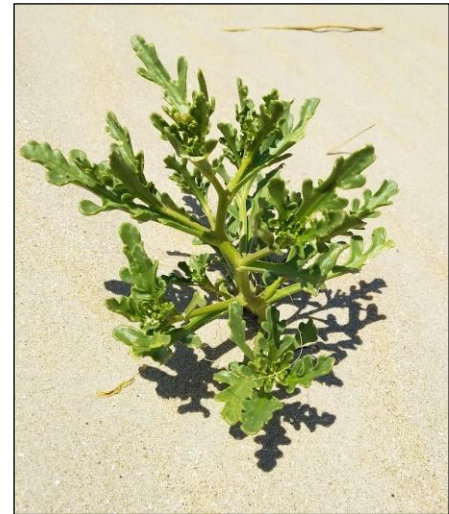


Figure 26: Pioneer *Cakile maritima* found at the edge of a deposition lobe, landwards of the foredune.

thesis still must be optimized much more before it can be used for reliable vegetation mapping, there are many possible applications once it is ready for them.

Firstly, the CNN can be employed on other orthophotos of the Bloemendaal blowout complex to create a time series of vegetation changes after the blowouts' excavation. Orthoimagery collected in February and March is also available for 2015, 2017, 2019 and 2020, so without additional training for season-dependent vegetation changes the vegetation could be tracked over a period of 7 years. Additionally, if the CNN was trained to recognize vegetation throughout different seasons, orthophotos going back to 2013 with at least one per year could be used to follow vegetation changes starting right after the blowout complex was fully excavated. This would both benefit the scientific knowledge about large-scale coastal dune vegetation response to disturbances, and provide information for effective coastal dune management.

Beyond Bloemendaal, the CNN could be applied to other Dutch coastal dune systems. Via PDOK ([www.pdok.nl](http://www.pdok.nl)), annual RGB orthophotos of the Netherlands (including all coastal dune areas) with resolutions of 25 by 25 cm (since 2016) and 8 by 8 cm (since 2021) are publicly available. Although the CNN would need further training to recognize more different types of vegetation and dune slacks properly, in the future it could possibly be used to provide a vegetation map of the entire Dutch dune system. This could be used to distinguish country-wide vegetation patterns and trends depending on e.g. nitrogen deposition, grazing pressure, visitor counts or chemical sand composition.

## 6. CONCLUSION

The main accomplishment in this thesis is the development of a CNN capable of classifying coastal dune vegetation from high-resolution RGB orthoimagery, achieving an overall accuracy of 75.8%. To my knowledge, this is the first CNN specifically developed for mapping coastal dune vegetation. The CNN is able to recognize the main vegetation classes found in the coastal dunes, corresponding to Natura 2000 habitat types, which makes it potentially useful for ecological studies and nature management. Although this CNN's overall accuracy should be optimized further to reduce the 24.2% misclassifications, a future CNN could be used for vegetation time-series and large-scale vegetation maps as well. This would make it a highly valuable tool in understanding coastal dune dynamics.

To improve the CNN's accuracy, the reference data could be expanded to include more classes, in particular the classes 'water' and 'grass-encroached vegetation' which were missing in the present CNN. On the other hand, elevation data can be excluded in future CNNs as it was not found to significantly improve CNN accuracy, presumably because there was no clear relationship between elevation and vegetation type. Furthermore, reference data could be adjusted to have a better balance between the different classes, as a positive relationship was found between a class's surface area in the reference data and the CNN's performance for that class. Finally, with better hardware, input tile size could be increased more, which was found to increase accuracy by reducing the CNN's misclassifications that were observed mainly close to tile edges and borders.

In general, the efficiency with which a CNN can map vegetation from relatively accessible RGB orthoimagery could have a large impact on the field of ecology. It is still a very young field, and developments are following each other up quickly. As coastal dune ecosystems are deteriorating under high levels of stress, and measures are taken to recover them, it is very important to understand how coastal dune vegetation responds to stress and disturbances, also on long timescales and over large areas. Hopefully, CNN will be able to help us understand this better in the future, and aid in restoring and protecting the coastal dune ecosystem from further threats.

## REFERENCES

- Allaire, J. J., & Chollet, F. (2022). *keras: R Interface to "Keras."* <https://cran.r-project.org/package=keras>
- Allaire, J. J., & Tang, Y. (2022). *tensorflow: R Interface to "TensorFlow."* <https://cran.r-project.org/package=tensorflow>
- Alloghani, M., Al-Jumeily, D., Mustafina, J., Hussain, A., & Aljaaf, A. J. (2020). *A Systematic Review on Supervised and Unsupervised Machine Learning Algorithms for Data Science*. 3–21. [https://doi.org/10.1007/978-3-030-22475-2\\_1](https://doi.org/10.1007/978-3-030-22475-2_1)
- Arens, S. M., Mulder, J. P. M., Slings, Q. L., Geelen, L. H. W. T., & Damsma, P. (2013). Dynamic dune management, integrating objectives of nature development and coastal safety: Examples from the Netherlands. *Geomorphology*, *199*, 205–213. <https://doi.org/10.1016/J.GEOMORPH.2012.10.034>
- Arens, S. M., Slings, Q. L., Geelen, L. H. W. T., & Van der Hagen, H. G. J. M. (2013). Restoration of Dune Mobility in The Netherlands. *Restoration of Coastal Dunes*, 107–124. [https://doi.org/10.1007/978-3-642-33445-0\\_7](https://doi.org/10.1007/978-3-642-33445-0_7)
- Ayrey, E., & Hayes, D. J. (2018). The Use of Three-Dimensional Convolutional Neural Networks to Interpret LiDAR for Forest Inventory. *Remote Sensing*, *10*(4), 649. <https://doi.org/10.3390/RS10040649>
- Barbosa, A., Trevisan, R., Hovakimyan, N., & Martin, N. F. (2020). Modeling yield response to crop management using convolutional neural networks. *Computers and Electronics in Agriculture*, *170*, 105197. <https://doi.org/10.1016/J.COMPAG.2019.105197>
- Chen, C. H., Lin, P. H., Hsieh, J. G., Cheng, S. L., & Jeng, J. H. (2020). Robust multi-class classification using linearly scored categorical cross-entropy. *Proceedings of the 3rd IEEE International Conference on Knowledge Innovation and Invention 2020, ICKII 2020*, 200–203. <https://doi.org/10.1109/ICKII50300.2020.9318835>
- Clausing, G., Vickers, K., & Kadereit, J. W. (2000). Historical biogeography in a linear system: genetic variation of Sea Rocket (*Cakile maritima*) and Sea Holly (*Eryngium maritimum*) along European coasts. *Molecular Ecology*, *9*(11), 1823–1833. <https://doi.org/10.1046/J.1365-294X.2000.01083.X>
- Corenblit, D., Baas, A., Balke, T., Bouma, T., Fromard, F., Garófano-Gómez, V., González, E., Gurnell, A. M., Hortobágyi, B., Julien, F., Kim, D., Lambs, L., Stallins, J. A., Steiger, J., Tabacchi, E., & Walcker, R. (2015). Engineer pioneer plants respond to and affect geomorphic constraints similarly along water–terrestrial interfaces world-wide. *Global Ecology and Biogeography*, *24*(12), 1363–1376. <https://doi.org/10.1111/GEB.12373>
- Corenblit, D., Tabacchi, E., Steiger, J., & Gurnell, A. M. (2007). Reciprocal interactions and adjustments between fluvial landforms and vegetation dynamics in river corridors: A review of complementary approaches. *Earth-Science Reviews*, *84*(1–2), 56–86. <https://doi.org/10.1016/J.EARSCIREV.2007.05.004>
- Council of the European Commission. (1992). Council Directive 92/43/EEC of 21 May 1992 on the conservation of natural habitats and of wild fauna and flora. *Official Journal of the European Communities. Series L*, *206*, 7–50. [https://brestnatura.org/media/filer\\_public/06/01/060159e6-](https://brestnatura.org/media/filer_public/06/01/060159e6-)

e45b-44eb-b2db-2bf3293e79bc/habitat\_directive\_1992.doc

- Davy, A. J., Scott, R., & Cordazzo, C. V. (2006). Biological flora of the British Isles: *Cakile maritima* Scop. *Journal of Ecology*, 94(3), 695–711. <https://doi.org/10.1111/J.1365-2745.2006.01131.X>
- Doing, H. (1988). *Landschapsoecologie van nederlandse kust*. Stichting Duinbehoud.
- Doing, H. (1995). Landscape ecology of the Dutch coast. *Journal of Coastal Conservation* 1995 1:2, 1(2), 145–172. <https://doi.org/10.1007/BF02905123>
- Drees, M. (2004). Epidemieën onder wilde konijnen en de gevolgen. *Vakblad Natuur Bos En Landschap*, 9–11. <https://edepot.wur.nl/114392>
- Duistermaat, L. (2020). *Heukels' Flora van Nederland* (24th ed.). Noordhoff.
- Eisma, D. (1968). Composition, origin and distribution of Dutch coastal sands between Hoek Van Holland and the island of Vlieland. *Netherlands Journal of Sea Research*, 4(2), 123–267. [https://doi.org/10.1016/0077-7579\(68\)90011-2](https://doi.org/10.1016/0077-7579(68)90011-2)
- Evans, D. (2012). Building the European Union's natura 2000 network. *Nature Conservation*, 1, 11–26. <https://doi.org/10.3897/natureconservation.1.1808>
- Everts, F. H., Jongman, M., Tolman, M. E., & de Vries, N. P. J. (2005). *Vegetatiekartering Kennemerduinen rapp. nr. 543*.
- Grootjans, A. P., Adema, E. B., Bekker, R. M., & Lammerts, E. J. (2004). *Why Young Coastal Dune Slacks Sustain a High Biodiversity*. 85–101. [https://doi.org/10.1007/978-3-540-74002-5\\_6](https://doi.org/10.1007/978-3-540-74002-5_6)
- Guidici, D., Clark, M. L., Wang, Q., Younan, N. H., López-Martínez, C., & Thenkabail, P. S. (2017). One-Dimensional Convolutional Neural Network Land-Cover Classification of Multi-Seasonal Hyperspectral Imagery in the San Francisco Bay Area, California. *Remote Sensing* 2017, Vol. 9, Page 629, 9(6), 629. <https://doi.org/10.3390/RS9060629>
- Hartling, S., Sagan, V., Sidike, P., Maimaitijiang, M., & Carron, J. (2019). Urban Tree Species Classification Using a WorldView-2/3 and LiDAR Data Fusion Approach and Deep Learning. *Sensors*, 19(6), 1284. <https://doi.org/10.3390/S19061284>
- Heslenfeld, P., Jungerius, P. D., & Klijn, J. A. (2008). European Coastal Dunes: Ecological Values, Threats, Opportunities and Policy Development. *Ecological Studies*, 171, 335–351. [https://doi.org/10.1007/978-3-540-74002-5\\_20](https://doi.org/10.1007/978-3-540-74002-5_20)
- Hesp, P. A. (1991). Ecological processes and plant adaptations on coastal dunes. *Journal of Arid Environments*, 21(2), 165–191. [https://doi.org/10.1016/S0140-1963\(18\)30681-5](https://doi.org/10.1016/S0140-1963(18)30681-5)
- Hesp, P. A. (2002). Foredunes and blowouts: initiation, geomorphology and dynamics. *Geomorphology*, 48(1–3), 245–268. [https://doi.org/10.1016/S0169-555X\(02\)00184-8](https://doi.org/10.1016/S0169-555X(02)00184-8)
- Hewett, D. G. (1985). Grazing and mowing as management tools on dunes. *Vegetatio*, 62, 441–447. [https://doi.org/10.1007/978-94-009-5524-0\\_49](https://doi.org/10.1007/978-94-009-5524-0_49)
- Hijmans, R. J. (2022). *raster: Geographic Data Analysis and Modeling*. <https://rspatial.org/raster>
- IJzer, J., van Zeeland, Y. R. A., Montizaan, M. G. E., Egberink, H. F., König, P., & van Geijlswijk, I. M. (2016). Rabbit Hemorrhagic Disease Virus-2 (RHDV2): bij de konijnen af. Introductie van een nieuw type virus in Nederland in 2015. *Tijdschrift Voor Diergeneeskunde*, 3, 24–29.

- Isermann, M. (2011). Patterns in Species Diversity during Succession of Coastal Dunes. *Journal of Coastal Research*, 27(4), 661–671. <https://doi.org/10.2112/JCOASTRES-D-09-00040.1>
- Isermann, M., Diekmann, M., & Heemann, S. (2007). Effects of the expansion by *Hippophaë rhamnoides* on plant species richness in coastal dunes. *Applied Vegetation Science*, 10(1), 33–42. <https://doi.org/10.1111/J.1654-109X.2007.TB00501.X>
- Isermann, M., Koehler, H., & Mühl, M. (2010). Interactive effects of rabbit grazing and environmental factors on plant species-richness on dunes of Norderney. *Journal of Coastal Conservation*, 14(2), 103–114. <https://doi.org/10.1007/S11852-009-0056-9/FIGURES/5>
- Kattenborn, T., Eichel, J., & Fassnacht, F. E. (2019). Convolutional Neural Networks enable efficient, accurate and fine-grained segmentation of plant species and communities from high-resolution UAV imagery. *Scientific Reports 2019 9:1*, 9(1), 1–9. <https://doi.org/10.1038/s41598-019-53797-9>
- Kattenborn, T., Eichel, J., Wisser, S., Burrows, L., Fassnacht, F. E., & Schmidtlein, S. (2020). Convolutional Neural Networks accurately predict cover fractions of plant species and communities in Unmanned Aerial Vehicle imagery. *Remote Sensing in Ecology and Conservation*, 6(4), 472–486. <https://doi.org/10.1002/RSE2.146>
- Kattenborn, T., Leitloff, J., Schiefer, F., & Hinz, S. (2021). Review on Convolutional Neural Networks (CNN) in vegetation remote sensing. *ISPRS Journal of Photogrammetry and Remote Sensing*, 173, 24–49. <https://doi.org/10.1016/J.ISPRSIPRS.2020.12.010>
- Kilibarda, M., Sekulic, A., Hengl, T., Pebesma, E., & Graeler, B. (2015). *meteo: Spatio-Temporal Analysis and Mapping of Meteorological Observations*. <http://meteo.r-forge.r-project.org/>
- Kingma, D. P., & Lei Ba, J. (2015). Adam: A Method for Stochastic Optimization. *ICLR*.
- Knauer, U., von Rekowski, C. S., Stecklina, M., Krokotsch, T., Minh, T. P., Hauffe, V., Kiliyas, D., Ehrhardt, I., Sagischewski, H., Chmara, S., & Seiffert, U. (2019). Tree Species Classification Based on Hybrid Ensembles of a Convolutional Neural Network (CNN) and Random Forest Classifiers. *Remote Sensing*, 11(23), 2788. <https://doi.org/10.3390/RS11232788>
- Kooijman, A. M., Arens, S. M., Postema, A. E. L., van Dalen, B. R., & Cammeraat, L. H. (2021). Lime-rich and lime-poor coastal dunes: Natural blowout activity differs with sensitivity to high N deposition through differences in P availability to the vegetation. *Science of The Total Environment*, 779, 146461. <https://doi.org/10.1016/J.SCITOTENV.2021.146461>
- Kooijman, A. M., van Til, M., Noordijk, E., Remke, E., & Kalbitz, K. (2017). Nitrogen deposition and grass encroachment in calcareous and acidic Grey dunes (H2130) in NW-Europe. *Biological Conservation*, 212, 406–415. <https://doi.org/10.1016/J.BIOCON.2016.08.009>
- Kuipers, M., Arens, S. M., & Ruessink, B. G. (2016). Grootschalig herstel van stuivende duinen. *De Levende Natuur*, 117(003), 90–93. <https://natuurtijdschriften.nl/pub/718337/>
- Lamoot, I., Meert, C., & Hoffmann, M. (2005). Habitat use of ponies and cattle foraging together in a coastal dune area. *Biological Conservation*, 122(4), 523–536. <https://doi.org/10.1016/J.BIOCON.2004.09.009>
- Laporte-Fauret, Q., Castelle, B., Michalet, R., Marieu, V., Bujan, S., & Rosebery, D. (2021). Morphological and ecological responses of a managed coastal sand dune to experimental notches. *Science of The Total Environment*, 782, 146813. <https://doi.org/10.1016/J.SCITOTENV.2021.146813>

- Lecun, Y., Bengio, Y., & Hinton, G. (2015). Deep learning. *Nature* 2015 521:7553, 521(7553), 436–444. <https://doi.org/10.1038/nature14539>
- LeCun, Y., Matan, O., Boser, B., Denker, J. S., Henderson, D., Howard, R. E., Hubbard, W., Jackel, L. D., & Baird, H. S. (1990). Handwritten zip code recognition with multilayer networks. *Proceedings - International Conference on Pattern Recognition*, 2, 35–40. <https://doi.org/10.1109/ICPR.1990.119325>
- Liao, C., Wang, J., Xie, Q., Baz, A. Al, Huang, X., Shang, J., & He, Y. (2020). Synergistic Use of Multi-Temporal RADARSAT-2 and VEN $\mu$ S Data for Crop Classification Based on 1D Convolutional Neural Network. *Remote Sensing*, 12(5), 832. <https://doi.org/10.3390/RS12050832>
- Lin, G., & Shen, W. (2018). Research on convolutional neural network based on improved Relu piecewise activation function. *Procedia Computer Science*, 131, 977–984. <https://doi.org/10.1016/J.PROCS.2018.04.239>
- Marcenò, C., Guarino, R., Loidi, J., Herrera, M., Isermann, M., Knollová, I., Tichý, L., Tzonev, R. T., Acosta, A. T. R., FitzPatrick, Ú., Iakushenko, D., Janssen, J. A. M., Jiménez-Alfaro, B., Kaçki, Z., Keizer-Sedláková, I., Kolomyichuk, V., Rodwell, J. S., Schaminée, J. H. J., Šilc, U., & Chytrý, M. (2018). Classification of European and Mediterranean coastal dune vegetation. *Applied Vegetation Science*, 21(3), 533–559. <https://doi.org/10.1111/AVSC.12379>
- Maun, M. A. (1998). Adaptations of plants to burial in coastal sand dunes. *Canadian Journal of Botany*, 76(5), 713–738. <https://doi.org/10.1139/B98-058>
- Medina Machín, A., Marcello, J., Hernández-Cordero, A. I., Martín Abasolo, J., & Eugenio, F. (2019). Vegetation species mapping in a coastal-dune ecosystem using high resolution satellite imagery. *GIScience & Remote Sensing*, 56(2), 210–232. <https://doi.org/10.1080/15481603.2018.1502910>
- Mizutani, H. (1994). The back propagation method for CNN. *Proceedings of IEEE International Symposium on Circuits and Systems - ISCAS '94*, 463–466. <https://doi.org/10.1109/ISCAS.1994.409626>
- Mühr, B., Eisenstein, L., Pinto, J. G., Knippertz, P., Mohr, S., & Kunz, M. (2022). *CEDIM Forensic Disaster Analysis Group (FDA): Winter storm series: Ylenia, Zeynep, Antonia (int: Dudley, Eunice, Franklin) - February 2022 (NW & Central Europe)*. <https://doi.org/10.5445/IR/1000143470>
- Mulder, J. P. M., Hommes, S., & Horstman, E. M. (2011). Implementation of coastal erosion management in the Netherlands. *Ocean & Coastal Management*, 54(12), 888–897. <https://doi.org/10.1016/J.OCECOAMAN.2011.06.009>
- Nevavuori, P., Narra, N., & Lipping, T. (2019). Crop yield prediction with deep convolutional neural networks. *Computers and Electronics in Agriculture*, 163, 104859. <https://doi.org/10.1016/J.COMPAG.2019.104859>
- Nezami, S., Khoramshahi, E., Nevalainen, O., Pölönen, I., & Honkavaara, E. (2020). Tree Species Classification of Drone Hyperspectral and RGB Imagery with Deep Learning Convolutional Neural Networks. *Remote Sensing*, 12(7), 1070. <https://doi.org/10.3390/RS12071070>
- Niculescu, S., Ienco, D., & Hanganu, J. (2018). *Application of deep learning of multi-temporal SENTINEL-1 images for the classification of coastal vegetation zone of the Danube Delta*. 42(3), 1311–1318. <https://doi.org/10.5194/isprs-archives-XLII-3-1311-2018>
- Oksanen, J., Simpson, G. L., Blanchet, F. G., Kindt, R., Legendre, P., Minchin, P. R., O'Hara, R. B., Solymos,

- P., Stevens, M. H. H., Szoecs, E., Wagner, H., Barbour, M., Bedward, M., Bolker, B., Borcard, D., Carvalho, G., Chirico, M., De Caceres, M., Durand, S., ... Weedon, J. (2022). *vegan: Community Ecology Package*. <https://github.com/vegandevs/vegan>
- Oost, A. P., Hoekstra, P., Wiersma, A., Flemming, B., Lammerts, E. J., Pejrup, M., Hofstede, J., van der Valk, B., Kiden, P., Bartholdy, J., van der Berg, M. W., Vos, P. C., de Vries, S., & Wang, Z. B. (2012). Barrier island management: Lessons from the past and directions for the future. *Ocean & Coastal Management*, *68*, 18–38. <https://doi.org/10.1016/J.OCECOAMAN.2012.07.010>
- Oscro, L. P., Junior, J. M., Ramos, A. P. M., Furuya, D. E. G., Santana, D. C., Teodoro, L. P. R., Gonçalves, W. N., Baio, F. H. R., Pistori, H., Junior, C. A. da S., & Teodoro, P. E. (2020). Leaf Nitrogen Concentration and Plant Height Prediction for Maize Using UAV-Based Multispectral Imagery and Machine Learning Techniques. *Remote Sensing*, *12*(19), 3237. <https://doi.org/10.3390/RS12193237>
- Over, J.-S. R., Ritchie, A. C., Kranenburg, C. J., Brown, J. A., Buscombe, D. D., Noble, T., Sherwood, C. R., Warrick, J. A., & Wernette, P. A. (2021). Processing coastal imagery with Agisoft Metashape Professional Edition, version 1.6—Structure from motion workflow documentation. In *U.S. Geological Survey Open-File Report*. <https://doi.org/10.3133/OFR20211039>
- Parsons, V. L. (2017). Stratified Sampling. *Wiley StatsRef: Statistics Reference Online*. <https://doi.org/10.1002/9781118445112.STAT05999.PUB2>
- Pebesma, E. (2018). Simple Features for R: Standardized Support for Spatial Vector Data. *The R Journal*, *10*(1), 439–446. <https://doi.org/10.32614/RJ-2018-009>
- Pedrotti, F. (2012). *Plant and vegetation mapping*. Springer Science & Business Media.
- Provoost, S., & Declerck, L. (2020). Early scrub development in De Westhoek coastal dunes (Belgium). *Folia Geobotanica*, *55*(4), 315–332. <https://doi.org/10.1007/S12224-020-09385-1/FIGURES/7>
- Provoost, S., Jones, M. L. M., & Edmondson, S. E. (2011). Changes in landscape and vegetation of coastal dunes in northwest Europe: A review. *Journal of Coastal Conservation*, *15*(1), 207–226. <https://doi.org/10.1007/S11852-009-0068-5/FIGURES/4>
- R Core Team. (2020). *R: A Language and Environment for Statistical Computing*. <https://www.r-project.org/>
- Rezaee, M., Mahdianpari, M., Zhang, Y., & Salehi, B. (2018). Deep Convolutional Neural Network for Complex Wetland Classification Using Optical Remote Sensing Imagery. *IEEE Journal of Selected Topics in Applied Earth Observations and Remote Sensing*, *11*(9), 3030–3039. <https://doi.org/10.1109/JSTARS.2018.2846178>
- Rijksoverheid. (2021). *Ontwerp Nationaal Water Programma 2022-2027*. <https://open.overheid.nl/repository/ronl-9c782270-d575-42f3-9716-cd6b8f342b5b/1/pdf/1-ontwerp-nationaal-water-programma-2022-2027.pdf>
- Ronneberger, O., Fischer, P., & Brox, T. (2015). U-Net: Convolutional Networks for Biomedical Image Segmentation. *Lecture Notes in Computer Science (Including Subseries Lecture Notes in Artificial Intelligence and Lecture Notes in Bioinformatics)*, *9351*, 234–241. [https://doi.org/10.1007/978-3-319-24574-4\\_28](https://doi.org/10.1007/978-3-319-24574-4_28)
- Ruessink, B. G., Arens, S. M., Kuipers, M., & Donker, J. J. A. (2018). Coastal dune dynamics in response to excavated foredune notches. *Aeolian Research*, *31*, 3–17.



<https://doi.org/10.1016/J.AEOLIA.2017.07.002>

- Schmidtlein, S., Tichý, L., Feilhauer, H., & Faude, U. (2010). A brute-force approach to vegetation classification. *Journal of Vegetation Science*, 21(6), 1162–1171. <https://doi.org/10.1111/J.1654-1103.2010.01221.X>
- Schwarz, C., Brinkkemper, J., & Ruessink, G. (2019). Feedbacks between Biotic and Abiotic Processes Governing the Development of Foredune Blowouts: A Review. *Journal of Marine Science and Engineering* 2019, Vol. 7, Page 2, 7(1), 2. <https://doi.org/10.3390/JMSE7010002>
- Shrestha, A., & Mahmood, A. (2019). Review of deep learning algorithms and architectures. *IEEE Access*, 7, 53040–53065. <https://doi.org/10.1109/ACCESS.2019.2912200>
- Silge, J., Chow, F., Kuhn, M., & Wickham, H. (2021). *rsample: General Resampling Infrastructure*. <https://cran.r-project.org/package=rsample>
- Sothe, C., De Almeida, C. M., Schimalski, M. B., Liesenberg, V., La Rosa, L. E. C., Castro, J. D. B., & Feitosa, R. Q. (2020). A comparison of machine and deep-learning algorithms applied to multisource data for a subtropical forest area classification. *International Journal of Remote Sensing*, 41(5), 1943–1969. <https://doi.org/10.1080/01431161.2019.1681600>
- Suo, C., McGovern, E., & Gilmer, A. (2019). Coastal Dune Vegetation Mapping Using a Multispectral Sensor Mounted on an UAS. *Remote Sensing* 2019, Vol. 11, Page 1814, 11(15), 1814. <https://doi.org/10.3390/RS11151814>
- Tordoni, E., Bacaro, G., Weigelt, P., Cameletti, M., Janssen, J. A. M., Acosta, A. T. R., Bagella, S., Filigheddu, R., Bergmeier, E., Buckley, H. L., Ciccarelli, D., Forey, E., Hennekens, S. M., Lubke, R. A., Mahdavi, P., Peet, R. K., Peinado, M., Sciandrello, S., & Kreft, H. (2021). Disentangling native and alien plant diversity in coastal sand dune ecosystems worldwide. *Journal of Vegetation Science*, 32(1), e12861. <https://doi.org/10.1111/JVS.12961>
- Touw, A., & Rubers, W. V. (1989). *De Nederlandse Bladmossen*. St. Uitg. KNNV.
- Valdés-Correcher, E., Rodriguez, E., Kemp, Y. J. M., Wassen, M. J., & Cromsigt, J. P. G. M. (2018). Comparing the impact of a grazing regime with European bison versus one with free-ranging cattle on coastal dune vegetation in the Netherlands. *Mammal Research*, 63(4), 455–466. <https://doi.org/10.1007/S13364-018-0373-1/TABLES/5>
- Van Boxel, J. H., Jungerius, P. D., Kieffer, N., & Hampele, N. (1997). Ecological effects of reactivation of artificially stabilized blowouts in coastal dunes. *Journal of Coastal Conservation*, 3(1), 57–62. <https://doi.org/10.1007/BF02908179>
- Van De Walle, R., Massol, F., Vandegheuchte, M. L., & Bonte, D. (2022). The distribution and impact of an invasive plant species (*Senecio inaequidens*) on a dune building engineer (*Calamagrostis arenaria*). *NeoBiota*, 72, 1–23. <https://doi.org/10.3897/NEOBIOTA.72.78511>
- van der Hagen, H. G. J. M., van Rooijen, N., & Schaminée, J. H. J. (2020). Forty years of rabbit influence on vegetation development in the coastal dunes of Meijendel, the Netherlands. *Proceedings of the 2017 Littoral Conference 'Change, Naturalness and People,'* 90–116. [https://www.researchgate.net/profile/Thomas-Smyth-2/publication/345669429\\_Proceedings\\_of\\_the\\_2017\\_Littoral\\_conference\\_'Change\\_Naturalness\\_and\\_People'/links/5faa5efc458515157bfc13f5/Proceedings-of-the-2017-Littoral-conference-Change-Naturalness-and-People.pdf#page=90](https://www.researchgate.net/profile/Thomas-Smyth-2/publication/345669429_Proceedings_of_the_2017_Littoral_conference_'Change_Naturalness_and_People'/links/5faa5efc458515157bfc13f5/Proceedings-of-the-2017-Littoral-conference-Change-Naturalness-and-People.pdf#page=90)

- van Dobben, H. F., Bobbink, R., Bal, D., & van Hinsberg, A. (2014). *Overview of critical loads for nitrogen deposition of Natura 2000 habitat types occurring in The Netherlands*. <https://library.wur.nl/WebQuery/wurpubs/reports/452440>
- Van Til, M., & Kooijman, A. (2007). Rapid improvement of grey dunes after shallow sod cutting. *Coastline Reports*, 7, 53–60.
- Veer, M. A. C. (1997). Nitrogen availability in relation to vegetation changes resulting from grass encroachment in Dutch dry dunes. *Journal of Coastal Conservation*, 3(1), 41–48. <https://doi.org/10.1007/BF02908178>
- Veer, M. A. C., & Kooijman, A. M. (1997). Effects of grass-encroachment on vegetation and soil in Dutch dry dune grasslands. *Plant and Soil*, 192(1), 119–128. <https://doi.org/10.1023/A:1004280300820>
- Verstrael, T. J. (1996). Research on breeding birds in Dutch dune areas. *Landscape and Urban Planning*, 34(3–4), 301–313. [https://doi.org/10.1016/0169-2046\(95\)00238-3](https://doi.org/10.1016/0169-2046(95)00238-3)
- WallisDeVries, M. F., & Raemakers, I. (2001). Does Extensive Grazing Benefit Butterflies in Coastal Dunes? *Restoration Ecology*, 9(2), 179–188. <https://doi.org/10.1046/J.1526-100X.2001.009002179.X>
- Wani, J. A., Sharma, S., Muzamil, M., Ahmed, S., Sharma, S., & Singh, S. (2022). Machine Learning and Deep Learning Based Computational Techniques in Automatic Agricultural Diseases Detection: Methodologies, Applications, and Challenges. *Archives of Computational Methods in Engineering*, 29(1), 641–677. <https://doi.org/10.1007/S11831-021-09588-5/TABLES/11>
- Xie, Y., Sha, Z., & Yu, M. (2008). Remote sensing imagery in vegetation mapping: a review. *Journal of Plant Ecology*, 1(1), 9–23. <https://doi.org/10.1093/JPE/RTM005>
- Zarnetske, P. L., Hacker, S. D., Seabloom, E. W., Ruggiero, P., Killian, J. R., Maddux, T. B., & Cox, D. (2012). Biophysical feedback mediates effects of invasive grasses on coastal dune shape. *Ecology*, 93(6), 1439–1450. <https://doi.org/10.1890/11-1112.1>
- Zhang, M., Lin, H., Wang, G., Sun, H., & Fu, J. (2018). Mapping Paddy Rice Using a Convolutional Neural Network (CNN) with Landsat 8 Datasets in the Dongting Lake Area, China. *Remote Sensing*, 10(11), 1840. <https://doi.org/10.3390/RS10111840>
- Zhong, L., Hu, L., & Zhou, H. (2019). Deep learning based multi-temporal crop classification. *Remote Sensing of Environment*, 221, 430–443. <https://doi.org/10.1016/J.RSE.2018.11.032>

# APPENDIX

## Appendix A: List of species observed during the vegetation survey

Species	Family	Frequency
<b>Bryophyta (mosses)</b>		
<i>Hypnum cupressiforme</i>	Hypnaceae	11
<i>Syntrichia ruralis</i>	Pottiaceae	10
<i>Tortella flavovirens</i>	Pottiaceae	2
<b>Polypodiopsida (ferns)</b>		
<i>Polypodium vulgare</i>	Polypodiaceae	2
<b>Angiosperms (flowering plants)</b>		
<b>Monocots (grasses and grass-like plants)</b>		
<i>Calam agrostis arenaria</i>	Poaceae	30
<i>Calamagrostis epigejos</i>	Poaceae	7
<i>Carex arenaria</i>	Cyperaceae	16
<b>Eudicots</b>		
<b>Shrubs</b>		
<i>Berberis vulgaris</i>	Berberidaceae	1
<i>Hippophae rhamnoides</i>	Elaeagnaceae	25
<i>Ligustrum vulgare</i>	Oleaceae	8
<i>Rubus caesius</i>	Rosaceae	19
<b>Herbs</b>		
<i>Anthriscus caucalis</i>	Apiaceae	1
<i>Cardamine hirsuta</i>	Brassicaceae	9
<i>Cerastium semidecandrum</i>	Caryophyllaceae	14
<i>Claytonia perfoliata</i>	Montiaceae	1
<i>Cynoglossum officinale</i>	Boraginaceae	1
<i>Erodium cicutarium</i>	Geraniaceae	8
<i>Fragaria vesca</i>	Rosaceae	2
<i>Galium sp.</i>	Rubiaceae	3
<i>Galium verum</i>	Rubiaceae	6
<i>Geranium molle</i>	Geraniaceae	7
<i>Glechoma hederacea</i>	Lamiaceae	3
<i>Jacobaea vulgaris</i>	Asteraceae	18
<i>Myosotis ramosissima</i>	Boraginaceae	8
<i>Plantago sp.</i>	Plantaginaceae	1
<i>Saxifraga tridactylites</i>	Saxifragaceae	4
<i>Senecio inaequidens</i>	Asteraceae	8
<i>Sonchus arvensis</i>	Asteraceae	1
<i>Stellaria media</i>	Caryophyllaceae	11
Unidentified herb	-	1

<b>Species</b>	<b>Family</b>	<b>Frequency</b>
<i>Urtica urens</i>	Urticaceae	1
<i>Veronica arvensis</i>	Plantaginaceae	4
<i>Vicia lathyroides</i>	Fabaceae	1
<i>Viola tricolor</i>	Violaceae	2